Brain, Behavior, & Immunity - Health 43 (2025) 100935

Contents lists available at ScienceDirect

Brain, Behavior, & Immunity - Health

journal homepage: www.editorialmanager.com/bbih/default.aspx

Inhibition of hippocampal interleukin-6 receptor-evoked signalling normalises long-term potentiation in dystrophin-deficient *mdx* mice

Kimberley A. Stephenson [a], Aaron Barron [b], Mark G. Rae [a], Dervla O'Malley [a,c,*]

[a] Department of Physiology, School of Medicine, University College Cork, Western Road, Cork, Ireland
[b] Department of Anatomy and Neuroscience, University College Cork, Western Road, Cork, Ireland
[c] APC Microbiome Ireland, University College Cork, Western Road, Cork, Ireland

ARTICLE INFO

Keywords:
Duchenne muscular dystrophy
Dystrophin
Hippocampus
Interleukin-6
Bioenergetics
Long-term potentiation

ABSTRACT

Duchenne muscular dystrophy (DMD), an X-linked neuromuscular disorder, characterised by progressive immobility, chronic inflammation and premature death, is caused by the loss of the mechano-transducing signalling molecule, dystrophin. In non-contracting cells, such as neurons, dystrophin is likely to have a functional role in synaptic plasticity, anchoring post-synaptic receptors. Dystrophin-expressing hippocampal neurons are key to cognitive functions such as emotions, learning and the consolidation of memories. In the context of disease-induced chronic inflammation, we have explored the role of the pleiotropic cytokine, interleukin (IL)-6 in hippocampal dysfunction using immunofluorescence, electrophysiology and metabolic measurements in dystrophic *mdx* mice. Hippocampal long-term potentiation (LTP) of the Schaffer collateral-CA1 projections was suppressed in *mdx* slices. Given the importance of mitochondria-generated ATP in synaptic plasticity, reduced maximal respiration in the CA1 region may impact upon this process. Consistent with a role for IL-6 in this observation, early LTP was suppressed in dystrophin-expressing wildtype slices exposed to IL-6. In dystrophic *mdx* mice, exposure to IL-6 suppressed mitochondrial-mediated basal metabolism in CA1, CA3 and DG hippocampal regions. Furthermore, blocking IL-6-mediated signalling by administering neutralising monoclonal IL-6 receptor antibodies intrathecally, normalised LTP in *mdx* mice. The impact of dystrophin loss from the hippocampus was associated with modified cellular bioenergetics, which underpin energy-driven processes such as the induction of LTP. The additional challenge of pathophysiological levels of IL-6 resulted in altered cellular bioenergetics, which may be key to cognitive deficits associated with the loss of dystrophin.

1. Introduction

Duchenne muscular dystrophy (DMD) is an X-linked fatal disease caused by mutations in the sarcolemma-spanning structural protein, dystrophin. Loss of functional dystrophin results in contraction-induced damage to muscle fibres, leading to inflammation, myophagocytosis (Tulangekar and Sztal, 2021), loss of mobility (McDonald et al., 2018), impaired respiratory function and premature death. DMD is also linked to cognitive impairment, developmental delays (Ricotti et al., 2016), poor communication skills, lower intelligence quotients (IQs) (Felisari et al., 2000; Nardes et al., 2012) and deficits in verbal, short-term and working memory (Chieffo et al., 2022; Hinton et al., 2007; Snow et al., 2013).

Dystrophic *mdx* mice recapitulate these symptoms, exhibiting a poor capacity to learn new tasks, and deficits in storing spatial memories (Chaussenot et al., 2015; Lopez et al., 2018; Vaillend et al., 1995, 2004; Verhaeg et al., 2024). Dp71, expressed in both neurons and glia, is the most prevalent dystrophin isoform in the brain (Haenggi et al., 2004; Tadayoni et al., 2012), whereas full-length Dp427 dystrophin is exclusively expressed in neurons, where it is functionally linked with synaptogenesis and receptor anchoring in the post-synaptic membrane (Brunig et al., 2002; Waite et al., 2009). Dystrophin plays an important role in clustering and stabilising inhibitory synapses (Anderson et al., 2002; Brunig et al., 2002; Knuesel et al., 1999), thereby facilitating inhibitory signal transduction (Kueh et al., 2008; Vaillend and Billard, 2002). One of the brain regions where dystrophin is expressed is the hippocampus, a structure critical for acquiring and encoding memories (Rae and O'Malley, 2016). Indeed, recent work has determined that ageing is an important contributary factor in the deterioration of spatial learning and long-term memory in *mdx* mice (Bagdatlioglu et al., 2020).

* Corresponding author. Department of Physiology, College of Medicine and Health, Western Gateway Building, University College Cork, Cork, Ireland.
E-mail address: d.omalley@ucc.ie (D. O'Malley).

https://doi.org/10.1016/j.bbih.2024.100935
Received 8 July 2024; Received in revised form 30 October 2024; Accepted 21 December 2024
Available online 23 December 2024

There is, however, disagreement as to role that dystrophin plays in hippocampal long term potentiation (LTP), the proposed mechanism by which activity-dependent changes in pre- and/or post-synaptic signalling modifies synaptic strength and underpins information storage (Bliss and Collingridge, 1993). No deficits in hippocampal NMDA-dependent LTP were detected in *mdx* mice in an early study (Sesay et al., 1996), whereas others detected enhanced hippocampal-dependent LTP in *mdx* mice which, curiously, was accompanied by deficits in long-term spatial memory and object recognition (Vaillend et al., 2004). Yet another study reported that LTP was blunted in the absence of dystrophin (Moore et al., 2002). Loss of dystrophin is linked to mitochondrial dysfunction in myocytes, which may precede chronic inflammation (Budzinska et al., 2021; Moore et al., 2020) and calcium dyshomeostasis (Mareedu et al., 2021) but little is known about the importance of dystrophin for neuronal bioenergetics, either at rest or during energy intensive processes of learning, such as LTP.

The pro-inflammatory cytokine, interleukin-6 (IL-6), which is elevated in plasma and muscle from *mdx* mice (Manning et al., 2014; Pelosi et al., 2015), suppresses LTP and post-tetanic potentiation (PTP) (Li et al., 1997; Tancredi et al., 2000), an early stage of synaptic plasticity involving changes in transmitter release from pre-synaptic terminals (Lauri et al., 2007). IL-6 can cross the blood brain barrier (Banks et al., 1994) which, in any case is leaky in *mdx* mice (Nico et al., 2003). Of note, forced expression of IL-6 in *mdx* mice more faithfully recapitulates human symptoms of DMD (Pelosi et al., 2015). Moreover, IL-6 modulates pathways associated with energetic metabolism (Mirabella et al., 2021). In the context of pro-inflammatory dystrophinopathies, we hypothesised that elevated levels of IL-6 would impact upon the tightly regulated signalling in the neurocircuitry of the hippocampus that underlies activity-dependent long-term changes in synaptic efficacy. The specific study objectives were to establish the impact of dystrophin loss on LTP and hippocampal bioenergetics and to determine the role of IL-6 in these deficits.

2. Methods and materials

2.1. Ethical approval

All animal experiments were approved and performed following guidelines set out by the Health Products Regulatory Authority (HPRA), Ireland and following project authorisation (AEI9130/P088), as well as individual authorisation (AEI9130/I303). Animals were euthanized in accordance with European Directive 2010/63/EU.

2.2. Animals and tissue collection

Breeding pairs of dystrophin-deficient C57BL/10ScSn-Dmd^{mdx}/J (mdx, dystrophic) and dystrophin-expressing wildtype C57BL/10ScSn (WT) controls were purchased from Jackson Laboratory (Bar Harbor, Maine, US). Breeding colonies were established and maintained in the Specific Pathogen Free (SPF) unit, Biological Services Unit, University College Cork, Ireland. As DMD is inherited in an x-linked recessive manner, it primarily affects males. Thus, weaned male mice were housed in individually ventilated cage with no more than four male littermates in each cage. Mice were kept under an artificial light/dark cycle (light between 06:00 and 18:00 h), with free access to drinking water and standard chow. Mice were provided with wood chip bedding and cardboard tubes for environmental enrichment. Room temperature of 22 ± 1 °C and humidity of 57 ± 2% were maintained. Mice between 8 and 14 weeks old were used for experiments.

Mice were anaesthetised (5% isoflurane in oxygen) prior to euthanasia by decapitation. Hippocampal tissue was excised and stored in cold HEPES-buffered saline solution (HBSS, in mM NaCl, 130; KCl 5.4; $MgCl_2$, 2; $CaCl_2$ 0.5; D-Glucose, 2 and HEPES, 10). For immunofluorescence on slices, whole brains were submerged in 4% paraformaldehyde fixative and cryoprotected in a 30% sucrose solution (Sigma-Aldrich, Missouri, USA) made up in 0.1 mM Phosphate Buffered Saline (PBS, 24 h @ 4 °C). Tissue was then flash frozen in liquid nitrogen and stored at −80 °C until cryo-sectioned (20 μm sections, CM1850, Leica, Germany) in Optimal Cutting Temperature (OCT) embedding medium (Thermofisher Scientific, Massachusetts, USA). Cryo-sectioned tissue was mounted onto positively charged glass slides (SuperFrost© Plus, VWR International, Pennsylvania, USA) prior to immunofluorescent staining.

2.3. Immunofluorescence and confocal microscopy

Age-matched WT and *mdx* mice were used for the immunofluorescent studies (n = 5 mice per group). Cryo-sectioned hippocampal slices (10 μm in thickness, Leica Biosystems, Wetzler, Germany) mounted on glass slides (VWR, Dublin 15, Ireland) were permeabilized with 0.1% Triton X-100 and blocked with 1% donkey serum (Sigma Aldrich, UK). Hippocampal slices were immunolabelled with antibodies against dystrophin (mouse anti MANDRA-1, 1:100, Abcam, Cambridge, UK), IL-6 (mouse, 1:250, Santa Cruz biotechnology, US) and IL-6 receptors (IL-6Rα, 1:250, Santa Cruz biotechnology, overnight at 4 °C). TRITC- anti-rabbit, FITC- anti-mouse or AlexaFluor488-anti-rabbit (1:250, Jackson Immunoresearch, PA, US, 2 h, room temperature) conjugated fluorophores were used, as appropriate, to visualise antibody expression. Tissue sections were mounted using Dako-fluorescent mounting medium containing DAPI (Agilent Pathology Solutions Santa Clara, California, USA). Images were captured using a FV10i -Olympus-confocal microscope with Fluoview software (FV10i-SW, Olympus Europe, Hamburg, Germany). No non-specific fluorescent immuno-tagging was detected in negative control experiments, where tissues were incubated with primary antibodies in the absence of secondary antibodies or secondary fluorophores alone.

Using a sampling scheme similar to that described previously (West et al., 1991), the Corrected Total Cell Fluorescence (CTCF) was calculated using Image J/Fiji (open-source image analysis software, https://fiji.sc/) according to the following formula: CTCF = integrated density – (area of selected cell x mean fluorescence of background readings). Two researchers (both blinded to the groups) conducted the analysis and a mean value was taken and compared between WT and *mdx* hippocampal slices.

2.4. Induction of hippocampal Long-Term Potentiation (LTP)

Whole brains were excised from WT and *mdx* mice (n = >3 per group) and placed in a slush of frozen, carbogenated (95% O_2, 5% CO_2) cutting solution comprising in mM (sucrose 100, HEPES 20, NaCl 50, KCl 3, NaH_2PO_4 1.25, $NaHCO_3$ 28, $CaCl_2$ 0.5, $MgCl_2$ 7 and D-glucose 5). Transverse slices (300 μm thick) were sectioned using a vibrotome (5100mz, Campden Instruments Ltd., UK) and transferred to a solution of 50:50 cutting solution and artificial cerebrospinal fluid (aCSF) comprising in mM (HEPES 20, NaCl 125, KCl 2.5, NaH_2PO_4 1.25, $NaHCO_3$ 25, $CaCl_2$ 2, $MgCl_2$ 1 and D-glucose 25). After 30 min in this solution, slices were then transferred to 100% carbogenated aCSF (23–25 °C) for at least 1 h prior to experimentation. Hippocampal slices were individually transferred to a recording chamber and continually superfused with oxygenated aCSF (2 ml/min) through a feedback-controlled temperature regulator (28 °C, ThermoClamp-1, Digitimer, UK).

A bipolar stimulating electrode was used to stimulate Schaffer-collateral axons projecting from the CA3 to CA1 hippocampal subfields to evoke field excitatory postsynaptic potentials (fEPSPs) in the *stratum radiatum* of CA1. fEPSPs were recorded using an aCSF-filled, low resistance (2–5 MΩ), monopolar borosilicate glass electrode (Model G150TF-4, Multichannel systems, Germany). After a stabilisation period (~1 h), an input/output curve was generated by evoking fEPSPs at 0.05Hz, with current stimulation intensity adjusted to evoke 50% of the maximal fEPSP response. Following a 20 minute control recording

period at the same stimulation frequency, four high frequency trains of stimuli (100Hz for 1 s, 60 s intervals) were applied to the slice. Subsequently, fEPSPs (evoked at 0.05Hz) were recorded for at least a further hour. For analysis, fEPSP slopes were normalised to 100% with respect to the mean slope of the fEPSPs recorded during the 20-min control period preceding induction of LTP. Post-high frequency stimulation fEPSPs were normalised to the same baseline.

2.5. Preparing hippocampal tissue punches for CA1, CA3 and DG regions for microplate-based respirometry

Using a similar protocol to the tissue preparation for electrophysiology, *ex vivo* coronal brain sections (220 μm in thickness) excised from WT (n= >7) and *mdx* (n= >7) mice were sectioned using a vibrotome (5100mz, Campden Instruments Ltd., UK) and transferred to carbogenated 100% aCSF at room temperature. Following a previously published protocol (Underwood et al., 2020), biopsy punches (0.5 mm diameter, reusable rapid punch biopsy kit, WPI Europe, Herfordshire, UK) from the CA1, CA3 and DG regions of WT and *mdx* mice were placed directly into the centre of each SeaHorse XFe96 Extracellular Flux Assay sensor cartridge well (Seahorse Bioscience, Billerica, MA). Adherence to wells pre-coated with poly-D-lysine (Sigma UK, 20 min, followed by H_20 rinse) was visually confirmed using a brightfield microscope. Hippocampal punches were maintained in aCSF (10 μl) with or without IL-6 (1 nM, 1 h). To account for possible hypoxia induced during the incubation period, the order of preparing WT or *mdx* biopsies was alternated.

2.6. Measurements of Oxygen Consumption Rates (OCR)

A Seahorse XF96 Extracellular Flux analyser (Seahorse Bioscience, Billerica, MA) was used to detect real-time changes in cellular oxygen consumption using solid-state fluorescent oxygen biosensors (Wu et al., 2007). 180 μl XF DMEM culture medium (containing in mM $MgSO_4$ 0.8, $CaCl_2$ 1.8, NaCl 143, KCl 5.4, NaH_2PO_4 0.91, HEPES 5, pH 7.4) supplemented with pyruvate (1 mM), glucose (20 mM) and glutamine (2 mM) was added to the hippocampal punches on the XF96 microplates and allowed to equilibrate (1 h at 37 °C). Three baseline measurements of OCR were taken prior to sequential injection of mitochondrial complex inhibitors into each well. Three OCR readings were taken after addition of oligomycin (25 μM) to inhibit ATP synthase, FCCP (2 μM) to uncouple the proton gradient, rotenone (1 μM) and antimycin A (1 μM) to inhibit to inhibit complex I and complex III, respectively. Working concentration titres for each inhibitor were optimised prior to the Seahorse XF96 mitochondrial stress analysis. OCRs were automatically calculated, recorded, and plotted by Seahorse XF96 Wave software (Desktop 2.3, Seahorse Bioscience, Billerica, MA, USA). Data were normalised for total protein content per well based on the mass of the hippocampal biopsies.

2.7. RNA extraction and preparation

Hippocampal tissue from WT and *mdx* mice was excised and stored in RNALater (24–48 h, Thermofisher Scientific, Massachusetts, USA) prior to being flash frozen in liquid nitrogen and stored at −80 °C. Total RNA was extracted by homogenization using a glass tissue grinder (Dounce tissue grinder, 1 ml) in the presence of Tripure Isolation Reagent (Roche Diagnostics Ltd., UK). This was followed by serial incubations with chloroform (Sigma-Aldrich, Missouri, USA) and iso-propanol (Sigma-Aldrich, Missouri, USA) and centrifugation steps. The quantity and purity of the RNA was then assessed by spectrophotometry using a Nanodrop 1000 (Thermofisher Scientific, Massachusetts, USA). The quality of the RNA was assessed using an agarose gel electrophoresis system (E-Gel© X, Invitrogen, California, USA).

2.8. Reverse transcription quantitative polymerase chain reaction

Hippocampal RNA from WT and *mdx* mice (n = 10 per group) was reverse transcribed using Transcriptor First Strand cDNA Synthesis Kit (Roche Diagnostics Ltd., UK). In brief, having determined total mRNA, the sample was diluted in diethyl pyrocarbonate-treated water to a final concentration of 200 ng. A template-primer mix (comprising 1 μg total RNA, anchored-oligo$(dT)_{18}$ primer (2.5 μM), random hexamer primer (60 μM), diethyl pyrocarbonate-treated water, Transcriptor Reverse Transcriptase Reaction Buffer (8 mM $MgCl_2$), protector RNAse inhibitor (20U/μl), deoxynucleotide mix (1 mM) and a Transcriptor Reverse Transcriptase (10 U)) was used to facilitate the reverse transcriptase reaction at 25 °C for 10 min, 55 °C for 30 min and 85 °C for 5 min. cDNA was amplified using Realtime ready Catalog or Designer Assays (Roche Diagnostics Ltd., UK) and Fast Start Essential DNA Probe Master (Roche Diagnostics Ltd., UK) using a LightCycler 96 (Roche Diagnostics Ltd., UK) on 96-well plates. All reactions were performed in duplicate, and reverse transcriptase negatives, RNA negatives, and cDNA negatives (with no template), and plate calibrator controls were included on every plate. Hippocampal gene expression of *Il6* (assay ID: 300699, configuration no.: 100138317), *Il6* receptor (assay ID: 300800, configuration no.: 100138308), *gp130* (assay ID: 314939, configuration no.: 100151248) and *STAT3* (assay ID: 316898, configuration no.: 100141760) were assessed and normalised to the reference gene, *HPRT1* (assay ID: 307879, configuration no.: 100140590). The relative expression of genes was calculated as ΔΔCT (normalised expression of the gene of interest to that of the reference gene, with changes in expression displayed as a fold change relative to the control group).

2.9. Enzyme-linked immunosorbent assay (ELISA)

To extract protein, WT and *mdx* hippocampal tissue (n = 10 WT vs 10 *mdx* mice) was homogenised using a glass tissue grinder (Dounce, 1 ml tissue grinder) in 500 μl lysis buffer (comprising Tris-HCl (10 mM, pH 7.0) Triton X-100 (0.5%), and cOmplete™, Mini, EDTA-free Protease Inhibitor Cocktail (Roche Diagnostics Ltd., UK) made up with Tris-HCL. Samples were centrifuged at 10,000 rpm for 10 min at 4 °C and samples of the supernatant were stored at −80 °C. An ELISA was performed using the LEGEND MAX™ Mouse IL-6 ELISA Kit (BioLegend, San Diego, USA). A standard curve was prepared using serial dilutions of standard IL-6 protein supplied with the kit. The ELISA plate was read at 570 nm and 450 nm using a multi well spectrophotometer (Molecular Devices, SpectraMax M3, USA).

2.10. Intervention study

WT and *mdx* mice (n = 3–5 per group) were randomly assigned to one of two groups (Fig. 8A). A single injection of saline (0.9% NaCl, 8 μl) or xIL-6R (MR16-1, Chugai Pharmaceutical Co., Ltd, Tokyo, Japan (Okazaki et al., 2002), 0.2 mg/kg body weight in volume of 8 μl saline) was administered intrathecally. Mice were anaesthetised (5% isoflurane in oxygen, Harvard Apparatus) and the hair from the lower lumbar region removed prior to intrathecal injection into the subarachnoid space between L5 and L6 using disposable 30-gauge sterile BD Microlance™ stainless steel needles (Becton Dickinson, New Jersey, USA) attached to a Hamilton™ 700 Microliter™ syringe (Luer tip, Hamilton, Reno, USA). Successful injection site was confirmed by observation of a tail flick. Mice were allowed to recover in a holding chamber (Thermacage, UK, 30 °C) and were kept under observation to confirm normal ambulation. They were returned to their home cage for 24 h prior to being euthanized to carry out electrophysiological assessment of LTP. Only datasets where LTP was successfully generated was included for analysis. The investigator was not blinded to the intervention groups while carrying out the experimental work, but subsequent analysis of the data was blinded.

2.11. Statistics

GraphPad Prism Version 8.4.2 (GraphPad Software Inc., USA) was used for statistical analyses. The data are represented as mean values ± standard deviation of the mean. Data were tested for normality and variance (Shapiro-Wilk test) and appropriate corrections were used. Statistical analysis was conducted on mean values with one animal taken as n = 1. Unpaired t-tests, one-way or two-way ANOVAs with post-hoc tests (Tukey's or Sidak's multiple comparisons) were used, where appropriate. $P \leq 0.05$ was considered significant.

3. Results

3.1. Dystrophin is absent from hippocampal tissue in dystrophic mdx mice

The full dystrophin isoform, Dp427, has been reported in pyramidal neuronal cell bodies of the CA1-CA3 hippocampal layers, whereas Dp71, the most prevalent isoform of dystrophin in the brain, has been detected in granule neurons of the dentate gyrus (Culligan and Ohlendieck, 2002), in addition to microglia and astrocytes. Using a primary antibody which detects both Dp427 and Dp71 isoforms (anti-MANDRA-1), distinct immunofluorescent labelling was detected in morphologically-identified cell bodies in the CA1 cell body layer (n = 4 mice) and CA3 (n = 4 mice) hippocampal regions and the granule cell layer of the dentate gyrus (DG, n = 5 mice) in dystrophin-expressing wildtype (WT) mice (Fig. 1A). The pattern of immunostaining was consistent with strongest expression at the plasma membranes of neuronal cell bodies in the CA1, CA3 and DG regions (inset, Fig. 1A). Consistent with *mdx* mice expressing a mutation that results in loss of dystrophin, semi-quantitative analysis of intensity of immunofluorescent staining in the neuronal cell layers demonstrated absence of dystrophin-positive immunostaining in CA1 ($p = 0.002$, n = 5 mice), CA3 ($p = 0.002$, n = 5 mice) and DG ($p < 0.025$, n = 5 mice) regions from matched *mdx* hippocampal slices (Fig. 1B and C). Specific

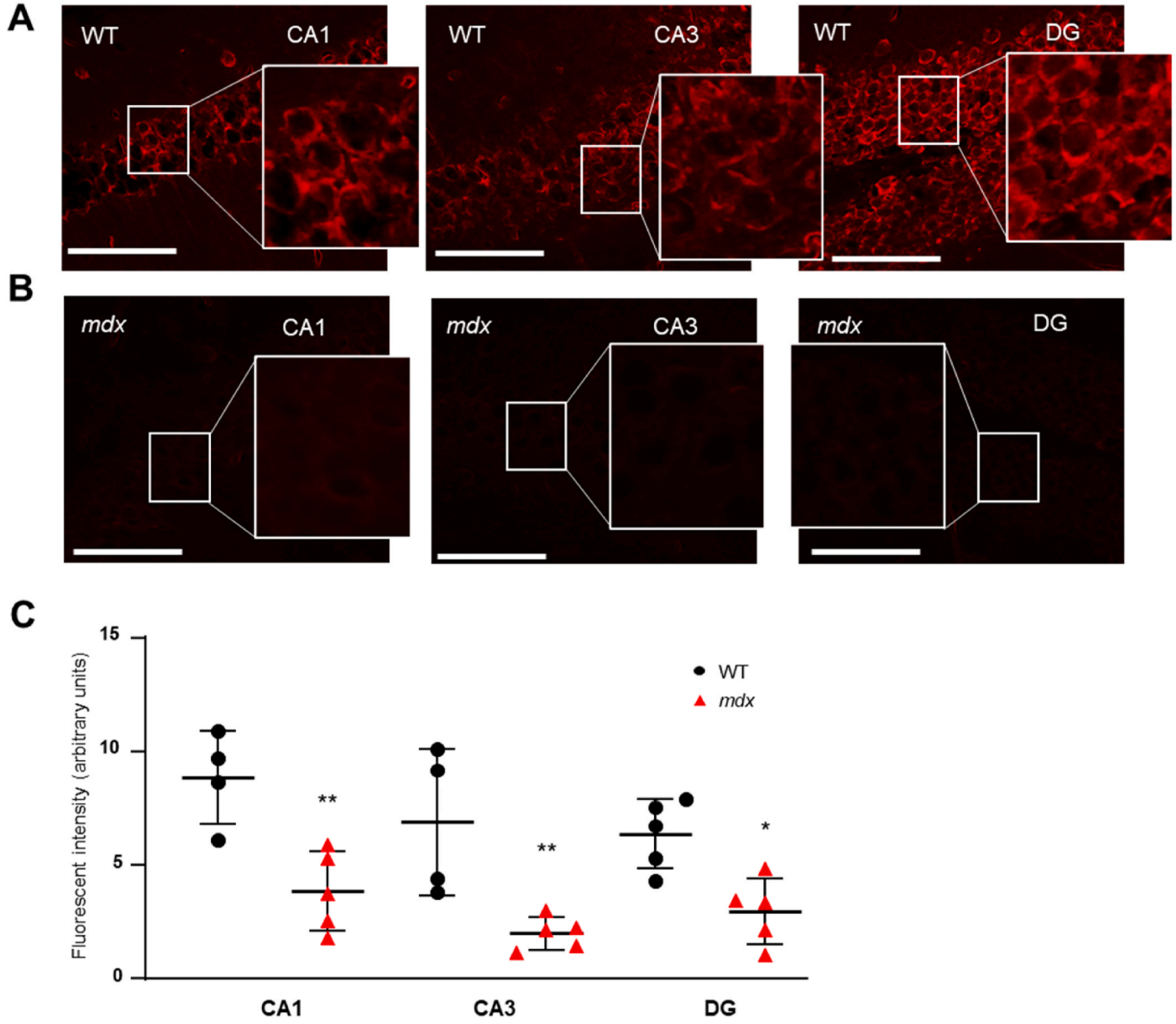

Fig. 1. Dystrophin is absent from CA1, CA3 and dentate gyrus (DG) regions of *mdx* hippocampal tissue.
Representative immunofluorescent images from **A:** wildtype (WT) and **B:** dystrophic *mdx* mice and **C:** semi-quantitative data plot (WT: black circles; *mdx*: red triangles) illustrate the intensity (corrected total cell fluorescence, CTCF) of dystrophin expression in the neuronal cell layers from CA1, CA3 and DG regions of hippocampal slices. Insets illustrate pattern of dystrophin staining in neurons in the cell body layers. ** and ** indicates $p < 0.05$ and $p < 0.01$, respectively. Scalebar: 30 μm. (For interpretation of the references to colour in this figure legend, the reader is referred to the Web version of this article.)

hippocampal regions were identified using DAPI co-staining which labelled nuclei in the cell body layers.

3.2. LTP is suppressed in mdx mice

LTP, the proposed molecular correlate of learning and the consolidation of memories, was generated by applying high frequency stimulation (HFS – 4 x 100 pulses, 100Hz for 1s/60s) to the SC-CA1 collaterals. Consistent with descriptions of post-tetanic potentiation (PTP), an early stage of synaptic plasticity involving changes in transmitter release from pre-synaptic terminals (Lauri et al., 2007), which is induced by large, localised increases in pre-synaptic intracellular calcium (Swandulla et al., 1991), a rapid but short-lived increase in the slope of field excitatory post-synaptic potentials (fEPSPs) was initially observed (within 5 min), followed by sustained long-lasting (>1 h) increase in the fEPSPs indicative of LTP (Fig. 2B).

The rising slope was used as a proportional indicator of the synaptic current. Consistent with post-synaptic localisation of dystrophin (Anderson et al., 2002; Knuesel et al., 1999), input/output curves, used as a measure of the efficiency of pre-synaptic neurotransmitter release, were similar in dystrophin-containing WT and dystrophic *mdx* hippocampal slices ($F(1, 8) = 0.23$, $p = 0.64$, Fig. 2A). However, when PTP (fEPSPs in the first 5 min post-HFS) was compared, the mean slope for *mdx* mice (167.8 ± 37.6%, n = 6) was significantly suppressed ($p = 0.005$) as compared to WT mice (231 ± 34.6%, n = 9, Fig. 2B). Furthermore, fEPSPs recorded for 60 min post-HFS, when NMDA-dependent mechanisms, excluding protein synthesis, contribute to LTP (Bliss and Collingridge, 2019), remained decreased in dystrophin-deficient *mdx* hippocampal slices ($F(1, 13) = 8.52$, $p = 0.01$, two-way ANOVA starting 1 min after stimulation, Fig. 2B).

3.3. Variability in oxygen consumption rates (OCR) in WT and mdx hippocampal regions

Learning-related processes of the hippocampus have a high energy demand and, as such, dysregulation of mitochondrial ATP generation may contribute to hippocampal dysfunction (Olesen et al., 2020). Using a Seahorse Bioscience XF96 Cell Mito Stress Test, we investigated the mitochondrial OCR in real time in *ex vivo* hippocampal tissue punches of the neuronal cell layers from CA1, CA3 and DG regions of WT and *mdx* hippocampal slices. Investigation of basal mitochondrial respiration in WT and *mdx* mice showed regionally-distinct differences in specific components of cellular respiration in CA1, CA3 and DG hippocampal regions (Fig. 3A, B, C, respectively).

Similar to the findings of others (Underwood et al., 2020), in WT mice, basal respiration (timepoints A1, A2 and A3) was not significantly different in CA1 (n = 10 tissue punches from 8 mice), CA3 (n = 8 tissue punches from 8 mice, or DG (n = 9 tissue punches from 8 mice) regions

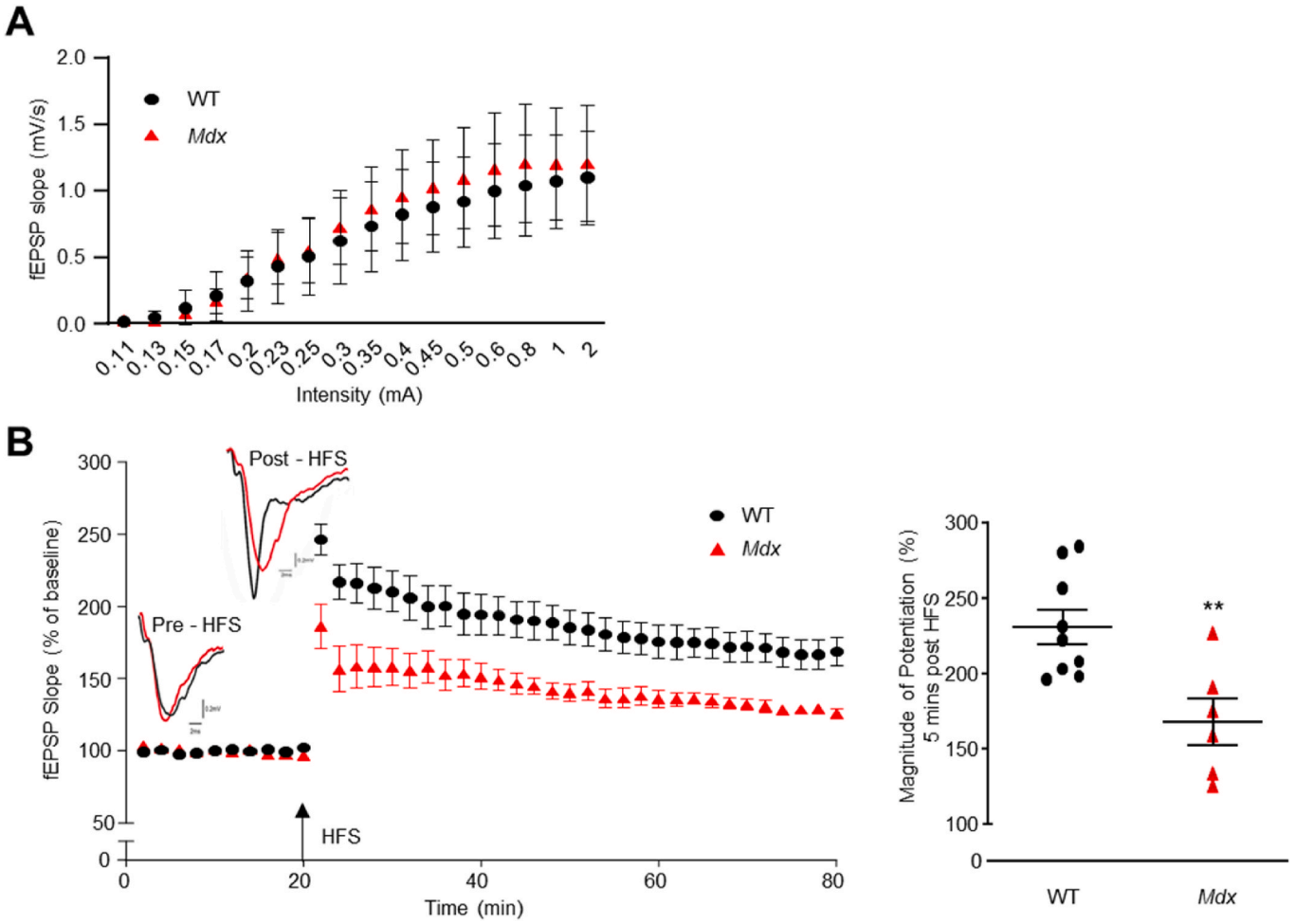

Fig. 2. Hippocampal long-term potentiation (LTP) is suppressed in *mdx* mice.
A: The hippocampal input/output (I/O) curve for wildtype (WT, black circles) and *mdx* (red triangles) mice prior to LTP induction were similar. **B:** The graph and representative sweeps (inset) show extracellular field excitatory post-synaptic potentials (fEPSPs) from CA1 *stratum radiatum* before and after tetanic high frequency stimulation (HFS) to induce LTP in WT and *mdx* mice. Pooled data of the amplitude of potentiation 5 min after HFS is shown for WT and *mdx* hippocampal slices. ** indicates $p < 0.01$. (For interpretation of the references to colour in this figure legend, the reader is referred to the Web version of this article.)

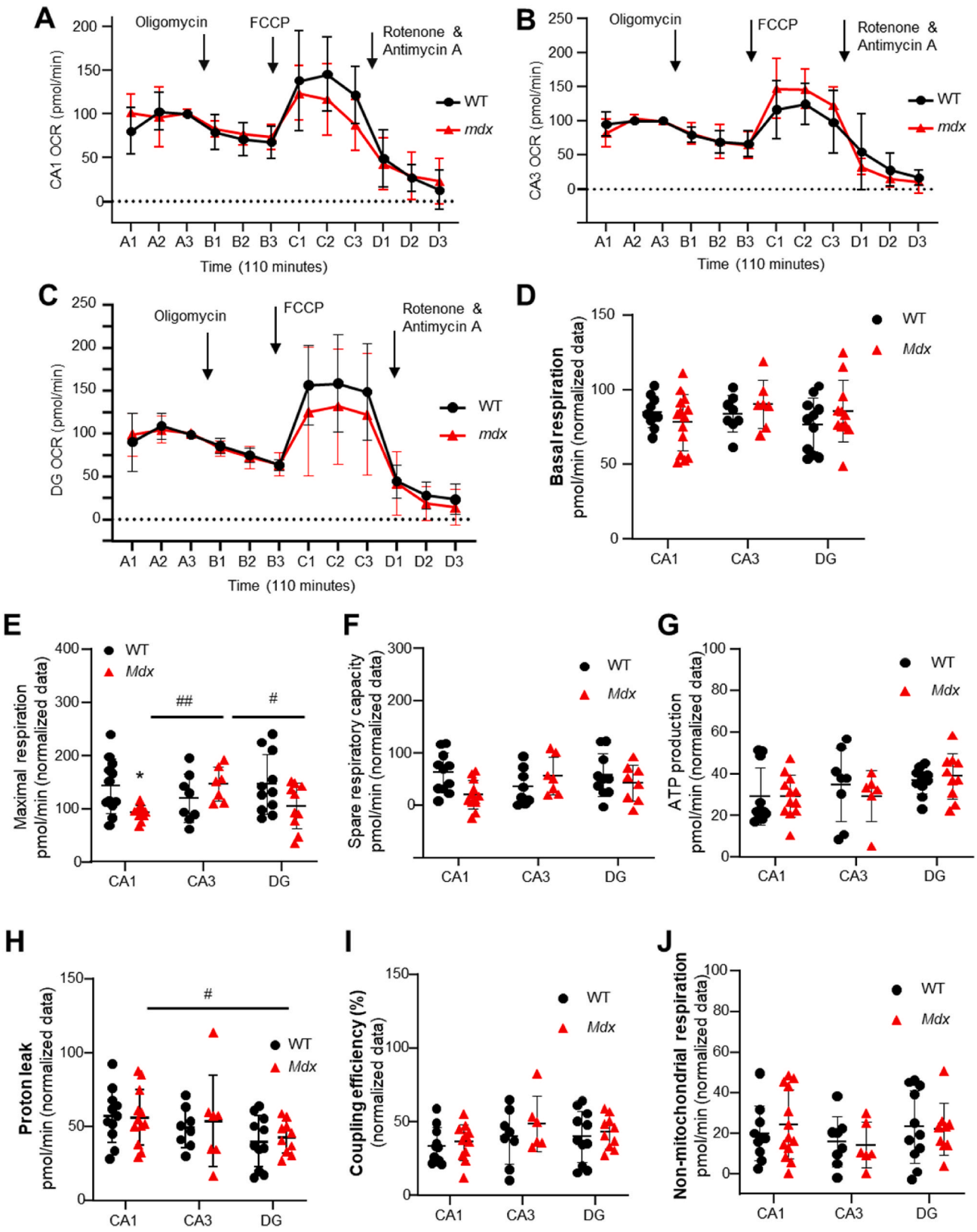

Fig. 3. Regional differences in bioenergetics were evident in WT and *mdx* hippocampal tissue.
The graphs illustrate real-time oxygen consumption rates (OCRs) over a period of 110 min in control wildtype (WT, black circles) and *mdx* (red triangles) hippocampal tissue punches from **A:** CA1; **B**: CA3 and **C**: DG regions. Time-response relationships for OCRs before and after addition of oligomycin, FCCP, and rotenone and antimycin A are illustrated with arrows for all groups. The data plots illustrate regional differences in **D:** basal respiration, **E:** maximal respiration, **F:** spare respiratory capacity, **G:** ATP production, **H:** proton leak, **I:** coupling efficiency and **J:** non-mitochondrial respiration in the CA1, CA3 and DG hippocampal regions from WT and *mdx* mice. * indicates $p < 0.05$ between strains. # and ## indicate $p < 0.05$ and $p < 0.01$ differences between brain regions. (For interpretation of the references to colour in this figure legend, the reader is referred to the Web version of this article.)

(Fig. 3D). Basal respiration was also comparable in CA1 (n = 11 tissue punches from 8 mice), CA3 (n = 7 tissue punches from 7 mice) and DG (n = 11 tissue punches from 8 mice) regions from dystrophic *mdx* hippocampal tissue ($F(2, 55) = 0.65$, $p = 0.52$, Fig. 5A). No strain differences were detected ($F(1, 55) = 0.41$, $p = 0.52$) and there was no interaction between the variables ($F(2, 55) = 1.47$, $p = 0.24$, Fig. 3D).

Maximal respiration (highest reading at C following application of FCCP, which uncouples mitochondrial oxidative phosphorylation, having subtracted lowest reading at D, Fig. 3A, B and C) is reported to be different in hippocampal regions (Underwood et al., 2020). Interestingly, our studies did not detect regional differences in WT tissue ($F(2, 29) = 0.68$, $p = 0.51$, Fig. 3E), but in *mdx* hippocampal tissues, we did observe increased maximal respiration in the CA3 region compared to CA1 ($p = 0.004$) and DG ($p = 0.03$) regions ($F2,25) = 6$, $p = 0.005$, one-way ANOVA, Fig. 3E). No overall differences were apparent between regions ($F(2, 53) = 0.57$, $p = 0.57$, two-way ANOVA) but strain

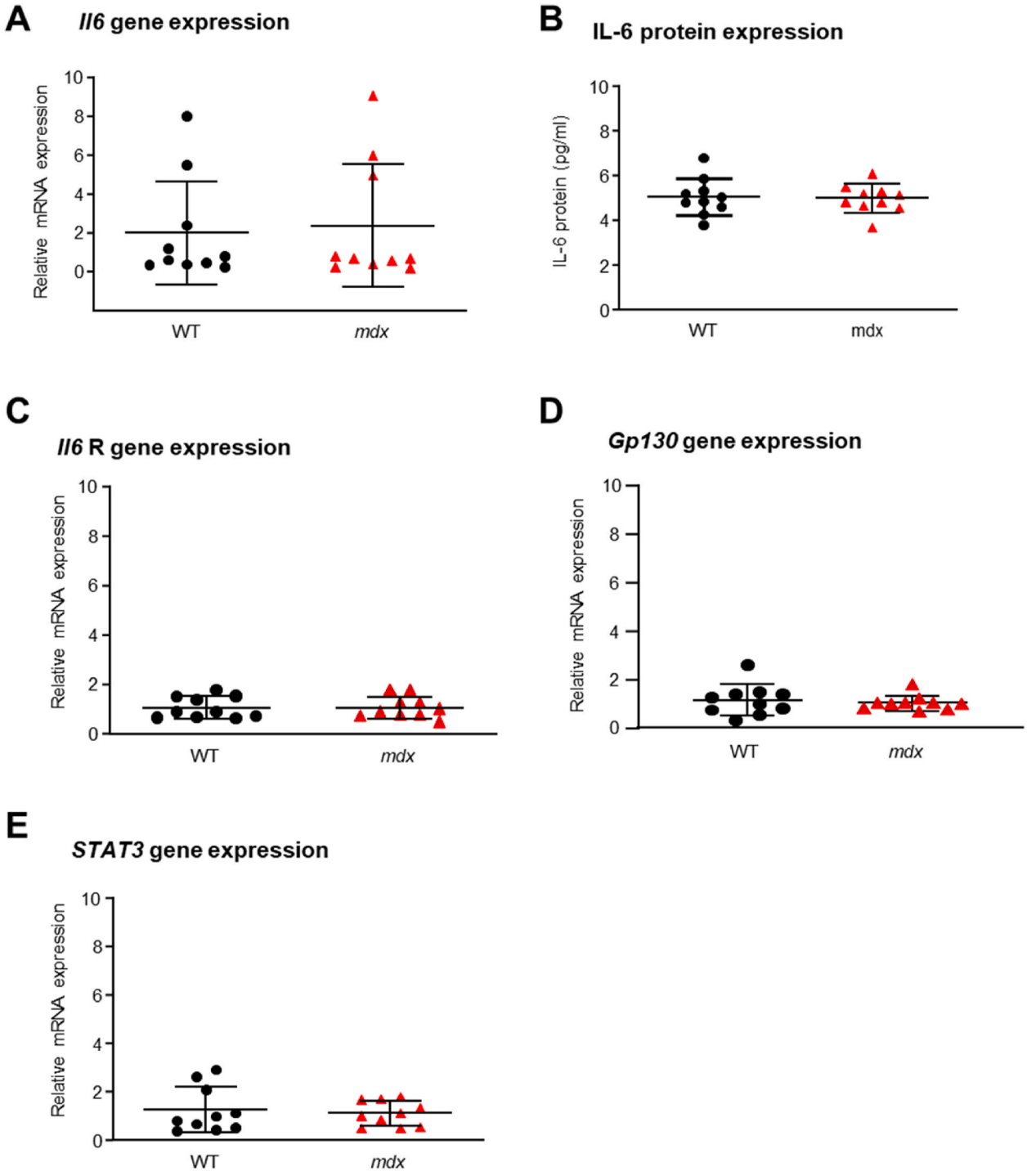

Fig. 4. Total interleukin-6 (IL-6) levels are similar in whole, homogenised wildtype (WT) and *mdx* hippocampal tissue.
A: Data plots indicate that the relative mRNA expression of *Il6* and **B:** protein expression of IL-6 was not different between hippocampal homogenates from wildtype (WT) and dystrophic *mdx* mice. **C:** Pooled data of relative mRNA expression of *Il6* receptors (*Il6* R) and **D:** the transmembrane glycoprotein, *gp130*, a signal transducing molecule for IL-6, are similar in WT and *mdx* hippocampal tissue. **E:** No difference was detected between groups in the relative gene expression for *STAT3*. $P > 0.05$ for all data sets.

differences approached significance ($F(1, 53) = 6.46$, $p = 0.07$), and decreased maximal respiration was detected in the CA1 region of *mdx* hippocampal tissue relative to WT ($p < 0.05$). A significant interaction between the maximal respiration in individual regions in each of the strains was detected ($F(2, 53) = 3.98$, $p = 0.025$).

Spare respiratory capacity is calculated from the difference between basal and maximal respiration values. Differences between CA1 and CA3 regions in *mdx* tissue approached significance ($p = 0.06$, one-way ANOVA, Fig. 3F). However, no overall regional ($F(2, 50) = 0.3$, $p = 0.74$) or strain effect ($F(1, 50) = 1.67$, $p = 0.2$, two-way ANOVA) was detected, although an interaction between strain and hippocampal region was present ($F(2, 50) = 3.6$, $p = 0.04$). ATP production was determined following addition of oligomycin (point A3, Fig. 3A, B and C), which inhibits oxidative phosphorylation of ADP to ATP. Overall, ATP production was not different between WT and *mdx* mice ($F(2, 52) = 0.1$, $p = 0.76$) but tended to be higher in the DG region of both strains ($F(2, 53) = 2.9$, $p = 0.065$, Fig. 3G). No interaction between variables was evident ($F(2, 52) = 0.42$, $p = 0.66$). Estimations of proton leak were lower in the DG compared to the CA1 region in both WT and *mdx* mice (Fig. 3H), resulting in a significant difference between hippocampal regions ($F(2, 53) = 3.84$, $p = 0.03$). No differences between strains were detected $F(1, 53) = 0.16$, $p = 0.69$) and no interaction between variables was evident $F(2, 52) = 0.12$, $p = 0.89$). The coupling efficiency (calculated as ATP production/basal respiration x 100) was not different between WT and *mdx* hippocampal tissue ($F(1,51) = 1.39$, $p = 0.24$) or between regions ($F(2,51) = 1.9$, $p = 0.15$) and no interaction between factors ($F(2,51) = 0.21$, $p = 0.81$) was evident (Fig. 3I). Non-mitochondrial oxygen consumption (component insensitive to rotenone A, an inhibitor of mitochondrial electron transfer, timepoints D1, D2 and D3, Fig. 3A, B and C) was also similar between hippocampal regions ($F(2, 51) = 1.3$, $p = 0.301$) and between WT and *mdx* mice ($F(1, 51) = 0.01$, $p = 0.92$) with no interaction between the variables ($F(2, 51) = 0.27$, $p = 0.76$, Fig. 3J).

3.4. Gene expression of IL-6 signalling pathway mediators are not altered in mdx hippocampal tissue

With elevated circulating IL-6 in dystrophic *mdx* mice (Pelosi et al., 2015), we explored if IL-6 was specifically increased in *mdx* hippocampal tissue. Under basal conditions, qRT-PCR was used to quantify gene expression of known components of the IL-6 signalling pathway. In homogenised whole hippocampal tissue, no differences in *Il-6* mRNA expression were evident between WT (2.0 ± 2.66, $n = 10$) and *mdx* (2.37 ± 3.16, $n = 10$) mice *($p = 0.78$,* Fig. 4A*)*. Although gene expression does not always correlate with protein expression *(*Liu et al., 2016*),* hippocampal IL-6 protein levels, determined using an IL-6 detection ELISA assay, were also comparable in WT (5.06 ± 0.83, $n = 10$) and *mdx* (4.98 ± 0.64, $n = 10$) hippocampal homogenates ($p = 0.81$, Fig. 4B). Furthermore, mRNA expression of *Il-6* receptors was similar in WT (1.078 ± 0.14, $n = 10$) and *mdx* (1.077 ± 0.14, $n = 10$) mice ($p = 0.99$, Fig. 4C), as was expression of *gp130*, the membrane-bound signal transducer for IL-6 in WT (1.16 ± 0.64, $n = 10$) and *mdx* (1.04 ± 0.31, $n = 10$) mice ($p = 0.61$, Fig. 4D). IL-6 is a key activator of Signal Transducer and Activator of Transcription (STAT) 3, a molecule critical to IL-6-mediated suppression of LTP (Tancredi et al., 2000). However, under basal conditions, no differences were detected in *STAT3* mRNA expression between WT (1.27 ± 0.94, $n = 10$) and *mdx* (1.12 ± 0.51, $n = 10$, $p = 0.65$, Fig. 4E) mice.

3.5. Region-specific changes in hippocampal IL-6 and IL-6R expression

As quantification of gene products in the IL-6 signalling cascade was compared using homogenised tissue from the whole hippocampus, this approach made it impossible to detect differences that were specific to CA1, CA3 and DG regions. However, using immunofluorescence we could semi-quantitatively compare mean fluorescent intensity of IL-6 and IL-6Rs in the cell body layers of these hippocampal regions, which were easily identified using DAPI nuclear labelling. In the pyramidal cell layers of CA1 and CA3 regions and granule cell layer of DG of both WT and *mdx* mice, diffuse IL-6 expression was apparent in the cytosol, with stronger, often punctate, staining near the cell membrane (Fig. 5A). The intensity of fluorescent staining of IL-6 was higher in the CA1 region of *mdx* (3.2 ± 1.24) compared to WT hippocampal tissue (*1.67 ± 0 0.66, $n = 5$ WT and 4 mdx mice,* $p = 0.048$, Fig. 5A). No difference in immunofluorescence intensity was detected in the CA3 region between WT (1.35 ± 0.56) and *mdx* (1.42 ± 1.16) mice ($n = 5$ WT and *mdx* mice, $p = 0.9$, Fig. 5A). IL-6 expression was higher in the *mdx* DG region (2.96 ± 1.44) in comparison to WT (0.89 ± 0.08, $n = 4$ WT and *mdx* mice, $p = 0.029$, Fig. 5A). Two-way ANOVA detected differences in IL-6 expression between the hippocampal regions ($F(2, 100) = 4.7$, $p = 0.01$) of *mdx* but not WT mice ($F(1, 100) = 9.7$, $p = 0.002$), with interaction between these factors ($F(2, 100) = 3.7$, $p = 0.03$). Thus, expression of neuronal IL-6 was elevated in the CA1 and DG regions of dystrophic hippocampal tissue.

IL-6R expression is primarily localised to the cell membrane of neurons in the CA1, CA3 and DG cell body layers of both mouse strains (Fig. 5B). The intensity of IL-6R immunofluorescent expression was increased in the CA1 region in *mdx* mice (12.31 ± 3.65) compared to WT mice (7.5 ± 1.8, $n = 5$ WT and *mdx* mice, $p = 0.03$, Fig. 5B). In contrast, IL-6R expression in the CA3 region was decreased in *mdx* mice (4.19 ± 2.1) compared to WT mice (8.5 ± 2.99, $n = 5$ WT and *mdx* mice, $p = 0.03$, Fig. 5B). In the DG, IL-6R expression was increased in *mdx* hippocampal tissue (4.4 ± 0.89), compared to WT (2.5 ± 1.19, $n = 5$ WT and 4 *mdx* mice, $p = 0.033$, Fig. 5B). Regional differences in IL-6R expression ($F(2, 69) = 26.6$, $p < 0.0001$, two-way ANOVA) were noted in both WT and *mdx* mice ($F(1, 69) = 2.07$, $p = 0.155$), and an interaction between the factors was detected ($F(2, 69) = 8.6$, $p = 0.0005$). Given the variability in IL-6R expression, sensitivity to IL-6 is likely to differ depending on the hippocampal region being stimulated.

3.6. IL-6-induced suppression of WT long-term potentiation (LTP) mimics LTP in mdx mice

Similar to previous reports that IL-6 can disrupt LTP (Tancredi et al., 2000), we observed that in-bath exposure of WT hippocampal slices to IL-6 (1 nM in aCSF 1 h prior to LTP and throughout recording protocol) resulted in suppression of PTP recordings (the first 5 min post-HFS) in WT hippocampal slices. Acute exposure to IL-6 supressed PTP ($177 \pm 25\%$, $n = 5$) as compared to control recordings ($231 \pm 35\%$, $n = 9$, $p = 0.01$, unpaired *t*-test, Fig. 6A). However, modulation of this early phase of potentiation in WT mice, did not endure over the longer duration of the recording ($F(1,12) = 0.05$, $p = 0.82$, two-way ANOVA starting 1 min after stimulation) between IL-6-and saline-treated WT mice. In contrast, LTP generated in dystrophic hippocampal slices, which was already suppressed in *mdx* hippocampal tissue (Fig. 2B), was not further modified by in-bath exposure to IL-6 (1 nM, 1 h prior to exposure and during recording protocol). The immediate PTP (first 5 min post HFS) was similar in *mdx* slices perfused with aCSF saline ($168 \pm 38\%$, $n = 6$) and *mdx* slices exposed to aCSF saline supplemented with IL-6 ($181 \pm 20\%$; $n = 5$, $p = 0.51$, Fig. 6B). Moreover, the fEPSP slopes were similar in the hour following the tetanic stimulus ($F(1,9) = 2.73$, $p = 0.133$, two-way ANOVA starting 1 min after stimulation). LTP in WT hippocampal slices exposed to IL-6 ($177 \pm 25\%$) was comparable to LTP in IL-6-exposed *mdx* mice ($181 \pm 20\%$; $p = 0.81$). However, it was interesting to observe that exposure to IL-6 in either WT or *mdx* hippocampal slices resulted in a notable increase in LTP stability, with more sustained LTP exhibiting less decay over the recording period.

3.7. IL-6 has region-specific effects on OCRs in WT and mdx hippocampal tissue

Region-specific changes in hippocampal OCRs were measured in

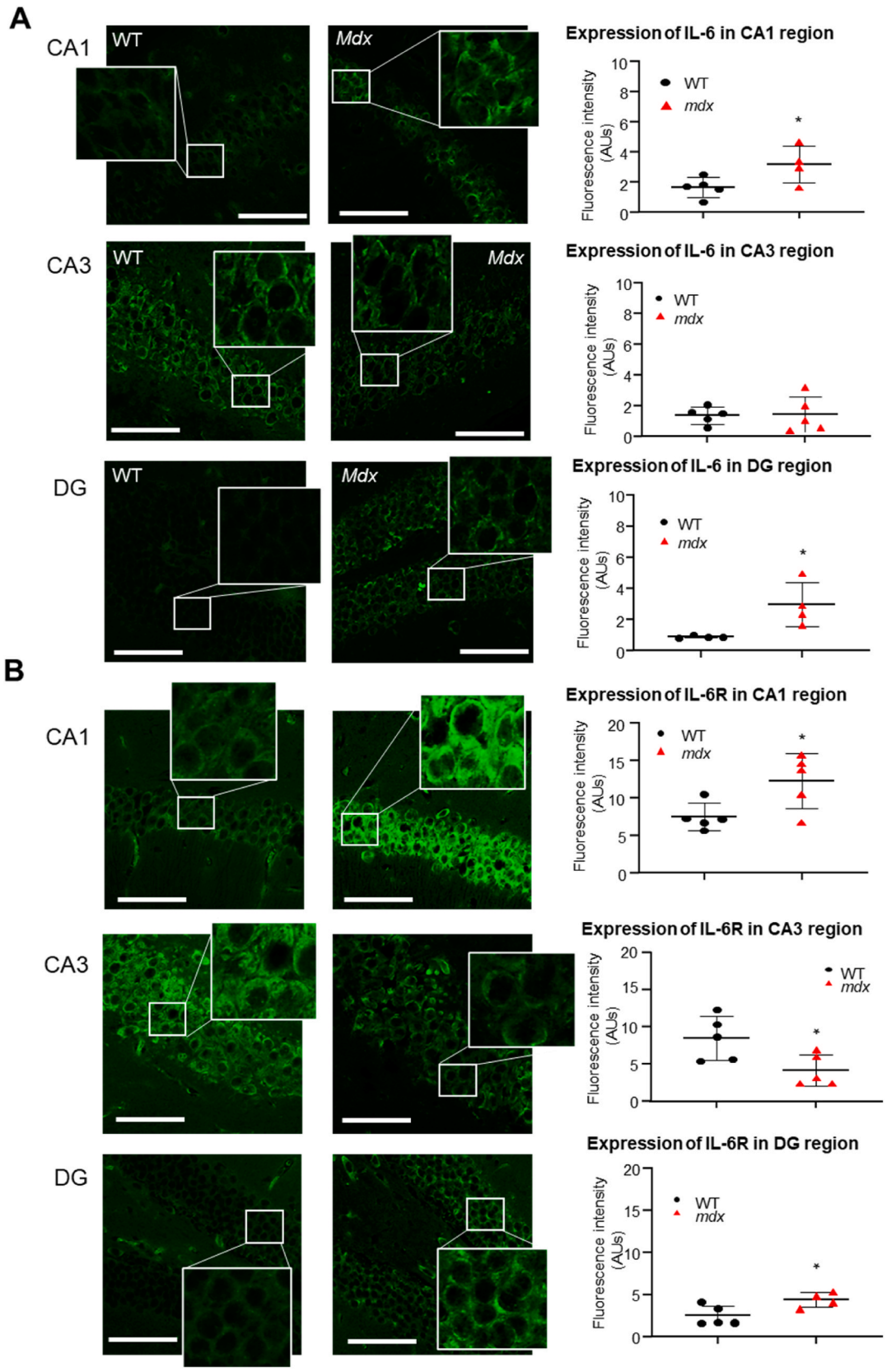

Fig. 5. Regionally distinct expression of hippocampal interleukin-6 (IL-6) and IL-6 receptors differs between WT and *mdx* mice.
Representative immunofluorescent images and data plots of corrected total cell fluorescence illustrate expression of **A:** IL-6 and **B:** IL-6 receptors in the neuronal cell layers of CA1, CA3 and DG hippocampal regions from wildtype (WT, black circles) and dystrophin-deficient, *mdx* (red triangles) mice. Insets show digitally magnified images of immuolabelled cell bodies. Scalebar: 70μm. * indicates $p < 0.05$. (For interpretation of the references to colour in this figure legend, the reader is referred to the Web version of this article.)

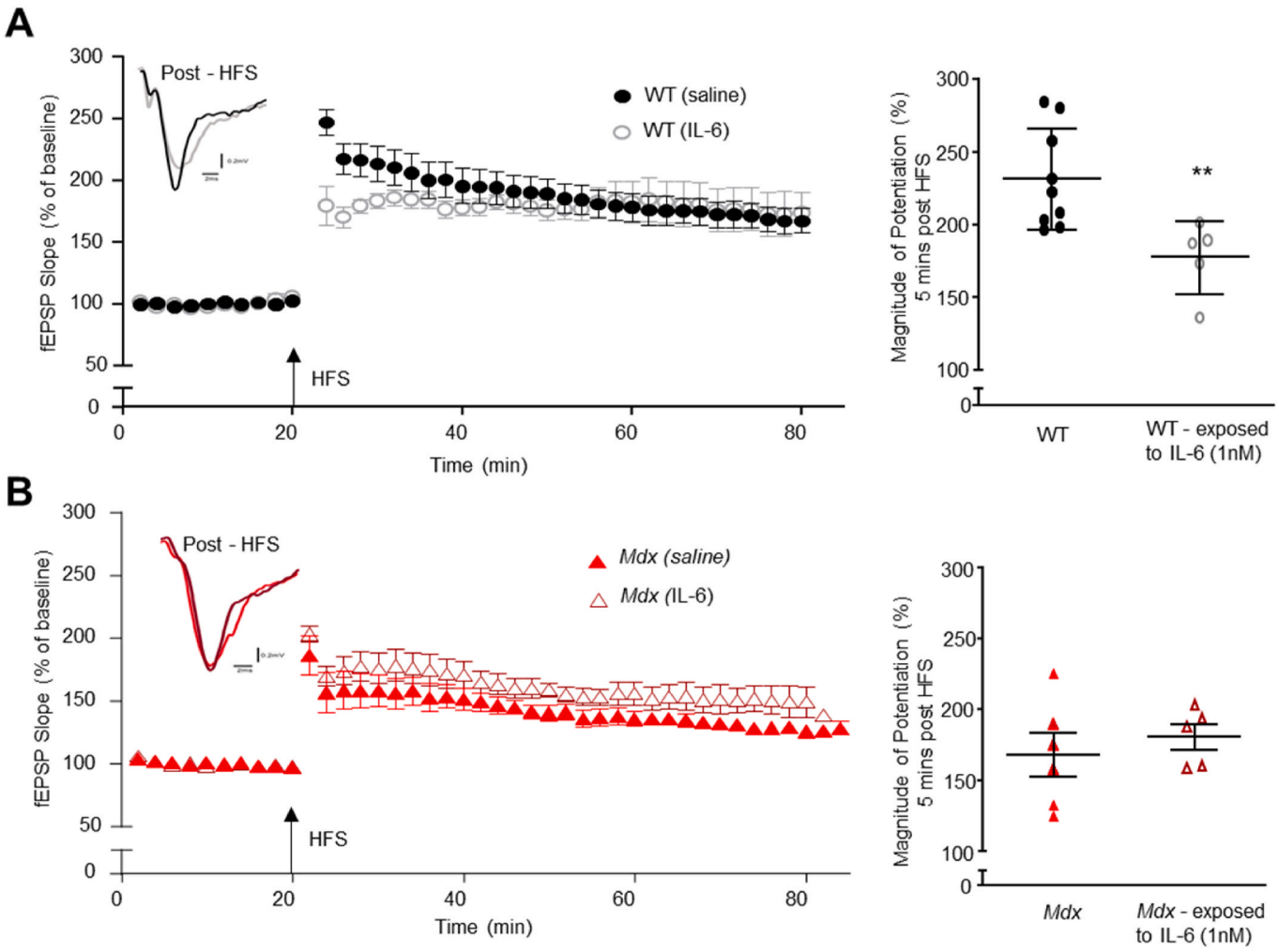

Fig. 6. Long-term potentiation (LTP) is suppressed in WT hippocampal slices exposed to interleukin (IL)-6.
The graphs and representative sweeps (inset) show fEPSPs before and after induction of LTP in **A:** WT mice or **B:** *mdx* mice under control (saline, solid shapes) conditions or following bath incubation with interleukin-6 (IL-6, 1 nM, >2 h, open shapes). Pooled data of the amplitude of potentiation 5 min after HFS is shown for WT and *mdx* hippocampal slices exposed to saline or IL-6. ** indicates $p < 0.01$.

tissues from WT (CA1: 12 biopsies from 8 mice, CA3: 7 biopsies from 7 mice and DG: 9 biopsies from 8 mice) and *mdx* (CA1: 12 biopsies from 8 mice, CA3: 11 biopsies from 7 mice and DG: 11 biopsies from 8 mice) hippocampal tissue acutely exposed to IL-6 (1 nM, >1 h, Fig. 7A, B and C). Under these conditions, basal respiration was lower in all three hippocampal regions in *mdx* relative to WT mice, revealing a significant strain effect ($F(1, 62) = 16.96$, $p = 0.001$) with no differences between regions ($F(2, 62) = 0.23$, $p = 0.8$) and an interaction between the variables approaching significance ($F(2, 62) = 0.06$, $p = 0.95$, Fig. 7D).

When exposed to IL-6, differences between maximal respiration in WT and *mdx* strains, noted in untreated tissue (Fig. 3E), were lost ($F(1, 59) = 1.16$, $p = 0.29$, Fig. 7E). Indeed, IL-6 suppressed maximal respiration in the WT CA3 region ($p = 0.04$). Regional differences in maximal respiration following IL-6 treatment approached significance ($F(2,59) = 2.8$, $p = 0.07$) but no interaction between the variables were detected ($F(2, 59) = 0.15$, $p = 0.86$, Fig. 7E). Spare respiratory capacity was not different between strains ($F(1, 58) = 0.01$, $p = 0.93$) or hippocampal regions ($F(2, 58) = 2.38$, $p = 0.1$) and the interaction between factors, which was evident in control tissue (Fig. 3F), was not observed following addition of IL-6 ($F(2, 58) = 0.98$, $p = 0.38$, Fig. 7F).

ATP production was similar in WT and *mdx* mice after IL-6 treatment ($F(1, 58) = 2.16$, $p = 0.15$), with similar levels in all hippocampal regions ($F(2, 58) = 0.02$, $p = 0.98$) and no interaction between variables ($F(2, 58) = 0.0005$, $p = 0.99$, Fig. 7G). Levels of proton leak were decreased in all *mdx* hippocampal regions, resulting in differences between the strains ($F(1, 63) = 5.37$, $p = 0.02$). However, no regional differences ($F(2, 63) = 0.61$, $p = 0.55$) or interaction between variables were evident ($F(2, 63) = 0.008$, $p = 0.99$, Fig. 7H). After exposure to IL-6, no strain ($F(1,58) = 0.29$, $p = 0.59$) or regional ($F(1,37) = 1.02$, $p = 0.32$) differences in coupling efficiency were detected but an interaction between these factors was detected ($F(2,58) = 3.4$, $p = 0.04$, Fig. 7I). Finally, we noted that non-mitochondrial oxygen consumption increased in *mdx* relative to WT hippocampal tissue ($F(1, 55) = 10.35$, $p = 0.002$), across all regions ($F(2, 55) = 0.68$, $p = 0.51$) after exposure to IL-6, with no interaction between factors ($F(2, 55) = 0.72$, $p = 0.49$, Fig. 7J).

Interestingly, when each region was examined individually, region-specific differences in cellular bioenergetics in the presence of IL-6 were evident. In the CA1 region, IL-6 suppressed basal respiration only in *mdx* tissue ($F(1, 47) = 7.8$, $p = 0.007$). Maximal respiration, which was reduced in saline-treated *mdx* tissue, remained suppressed following incubation with IL-6 ($F(1,43) = 12.28$, $p = 0.001$). Spare respiratory capacity in the CA1 region was suppressed in saline-exposed *mdx* tissue and that remained so after exposure to IL-6 ($F(1,43) = 7.8$, $p = 0.008$), indicating a difference between strains but no effect of the treatment *per se*. Proton leak ($F(1,47) = 1.9$, $p = 0.18$) was not significantly different in IL-6 treated tissue in this region. However, ATP production ($F(1,44) = 5.58$, $p = 0.02$) and coupling efficiency ($p =$

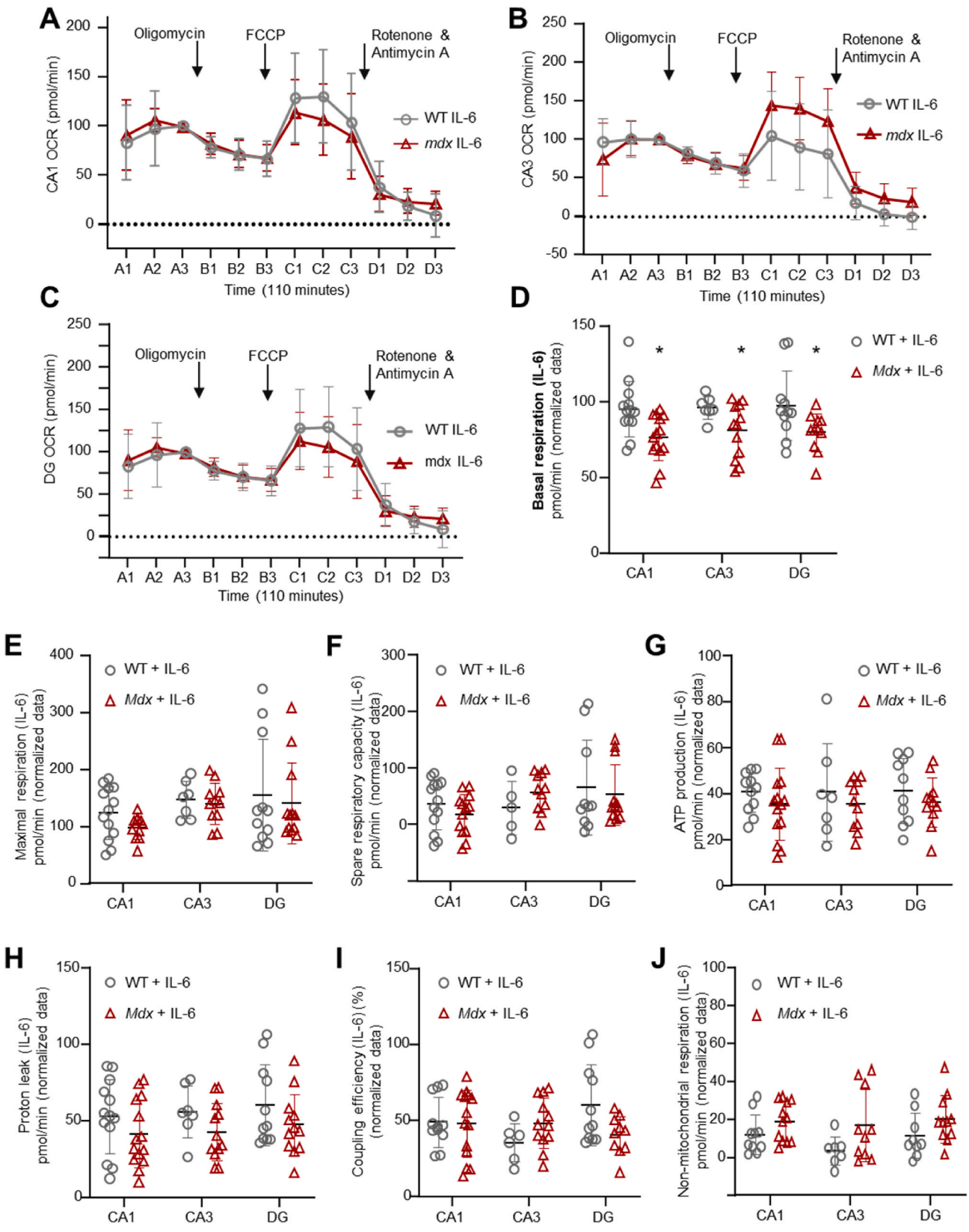

Fig. 7. Interleukin (IL) −6 suppressed basal mitochondrial respiration in *mdx* CA1, CA3 and DG hippocampal regions.
A: The graphs illustrate real-time oxygen consumption rates (OCRs) over a period of 110 min in wildtype (WT) and *mdx* hippocampal tissue punches from CA1; **B**: CA3 and **C**: DG cell body layers, which had been exposed to IL-6 (1 nM, 1 h). Time-response relationships for OCRs before and after addition of oligomycin, FCCP, and rotenone A and antimycin A are illustrated with arrows for all groups. The data plots illustrate regional differences in **D:** basal respiration, **E:** maximal respiration, **F:** spare respiratory capacity, **G:** ATP production, **H:** proton leak, **I:** coupling efficiency and **J:** non-mitochondrial respiration in the CA1, CA3 and DG hippocampal regions from IL-6- exposed tissue from WT and *mdx* mice. * indicates $p < 0.05$.

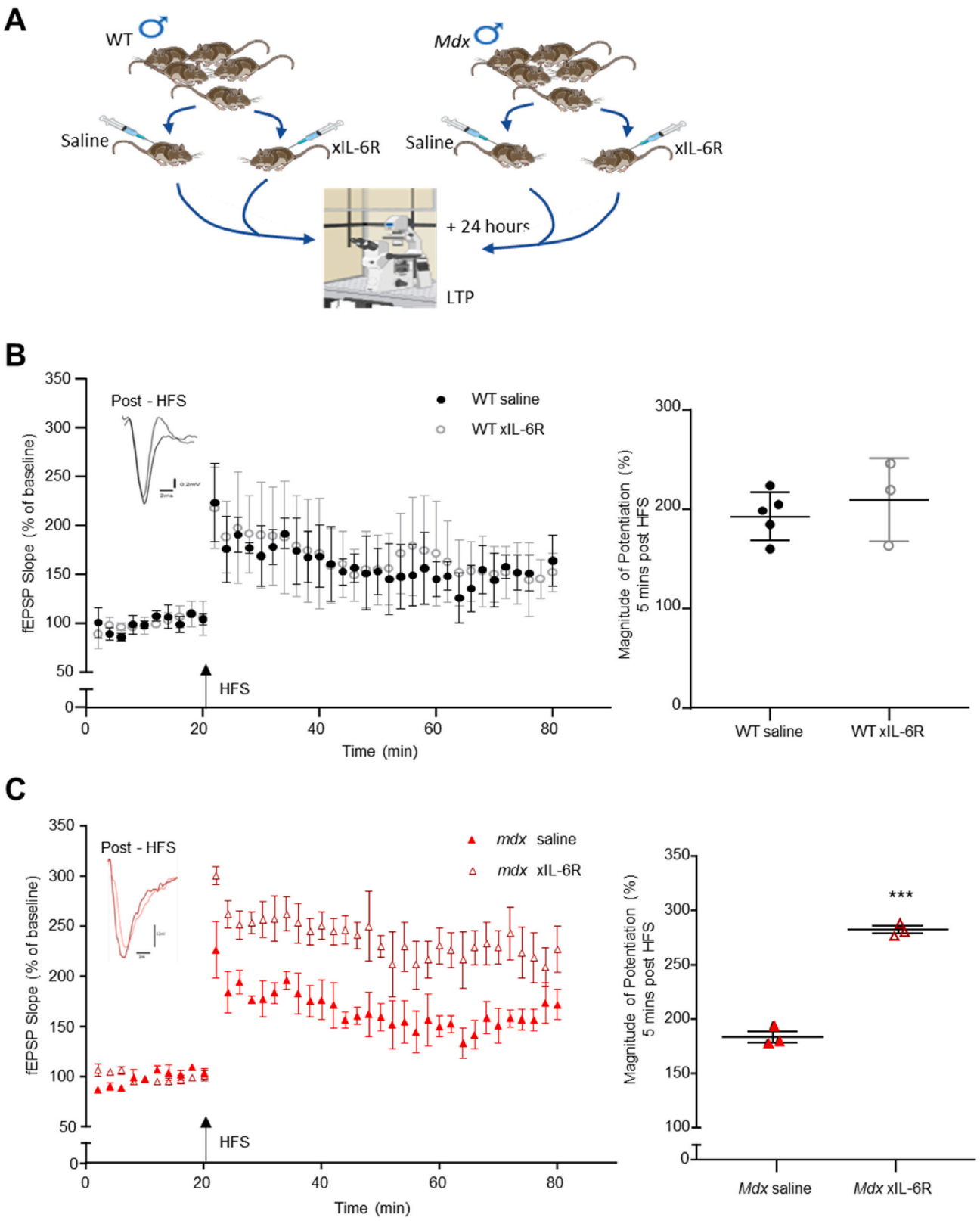

Fig. 8. Hippocampal long-term potentiation is normalised in *mdx* mice treated with neutralising monoclonal xIL-6R antibodies (xIL-6R).
A: The illustration outlines the protocol used for the intervention study. **B:** The graph and representative sweeps (inset) show extracellular field excitatory post-synaptic potentials (fEPSPs) from CA1 *stratum radiatum* in wildtype (WT) mice intrathecally injected with saline (black circles) and WT mice intrathecally administered xIL-6R (open grey circles) before and after tetanic high frequency stimulation (HFS, indicated by arrow) to induce LTP. **C:** The graph and representative sweeps (inset) show extracellular fEPSPs in *mdx* mice intrathecally injected with saline (solid red triangles) or xIL-6R (open red triangles) before and after tetanic HFS (indicated by arrow) to induce LTP. Pooled data of the amplitude of potentiation 5 min after HFS is shown for WT and *mdx* hippocampal slices following *in vivo* treatment with saline or xIL-6R monoclonal antibodies. *** indicates $p < 0.001$. (For interpretation of the references to colour in this figure legend, the reader is referred to the Web version of this article.)

0.008) was increased in both WT and *mdx* CA1 tissue following IL-6 exposure. No effect of IL-6 was observed on non-mitochondrial respiration ($F(1,41) = 2.66$, $p = 0.11$) in this region.

In the CA3 region, IL-6 increased basal respiration in WT tissue but decreased it in *mdx* tissue, resulting in an interaction between strain and treatment ($F(1,30) = 4.47$, $p = 0.04$). Maximal respiration remained elevated in IL-6-treated CA3 tissue, differing between the strains ($F(1, 29) = 5$, $p = 0.03$). However, there was no effect of incubation with IL-6 on spare respiratory capacity ($F(1,27) = 0.03$, $p = 0.87$), ATP production ($F(1,28) = 1.12$, $p = 0.3$), coupling efficiency ($F(1,28) = 0.16$, $p = 0.7$) or non-mitochondrial respiration ($F(1,27) = 0.84$, $p = 0.37$) in CA3 tissues.

In the DG region, an interaction between treatment with IL-6 and strain was evident in basal cellular respiration as levels were increased in WT DG tissue and decreased in *mdx* tissue ($F(1,40) = 5.53$, $p = 0.02$). There was no effect of IL-6 treatment on maximal respiration ($F(1,40) = 1.12$, $p = 0.3$), spare respiratory capacity ($F(1,36) = 0.27$, $p = 0.61$), ATP production ($F(1,38) = 0.07$, $p = 0.79$) or non-mitochondrial respiration ($F(1,37) = 1.02$, $p = 0.32$) in the DG gyrus region. However, IL-6 increased proton leak in DG tissue in both WT and *mdx* mice ($F(1,37) = 4.29$, $p = 0.045$). Moreover, IL-6 evoked enhanced coupling efficiency in WT but not *mdx* DG tissue, resulting in an interaction between strain and IL-6 treatment ($F(1,38) = 4.126$, $p = 0.049$).

3.8. Intrathecal administration of xIL-6R normalises long-term potentiation (LTP) in mdx mice

To further explore if IL-6 has a critical role in the suppression of LTP generated in SC-CA1 collaterals in *mdx* mice, neutralising monoclonal IL-6 receptor antibodies (xIL-6Rs) were intrathecally delivered *in vivo* to WT and *mdx* mice. In WT mice, 24 h after delivery of xIL-6Rs to the CNS (Fig. 8A), the mean slope of fEPSPs in the first 5 min post-HFS (209 ± 41.9%, $n = 3$) was comparable to WT mice administered saline (192.2 ± 24.1 %, $n = 5$, $p = 0.49$, Fig. 8B). Furthermore, fEPSPs recordings for 60 min post-HFS were not changed by the injection of xIL-6R in WT mice ($F(1, 3) = 5.02$, $p = 0.11$, two-way ANOVA starting 1 min after stimulation, Fig. 8B). In contrast, inhibition of central IL-6 signalling in *mdx* mice, through injection of xIL-6Rs, resulted in enhancement of LTP, compared to saline-injected *mdx* mice (Fig. 8C). The mean slope of fEPSPs in the first 5 min post-HFS in xIL-6R-injected *mdx* mice (282.3 ± 6.11%, $n = 3$) was greater than in *mdx* mice injected with saline (184.0 ± 8.72%, $n = 3$, $p < 0.0001$, Fig. 8C). Furthermore, fEPSPs recorded over the 60-min period post-HFS were enhanced in xIL-6R-treated *mdx* mice, as compared to saline-injected controls ($F(1, 4) = 12.19$, $p = 0.025$, two-way ANOVA, starting 1 min after stimulation). These results implicate the pleiotropic cytokine in the observed suppression of LTP associated with the loss of dystrophin.

4. Discussion

The hippocampus orchestrates spatially- and temporally-regulated neural pathways that encode and consolidate sensory input into enduring long-term memories (Knuesel et al., 2000; Lidov et al., 1990, 1993; Sekiguchi et al., 2009). Hippocampal pyramidal and granule cells are dystrophin-expressing populations of neurons important in cognitive processes related to emotions, learning and memory consolidation. In individuals with DMD, lacking the dystrophin protein, learning deficits are an early symptom of the condition (Felisari et al., 2000; Hinton et al., 2001; Nardes et al., 2012; Snow et al., 2013). In our studies, loss of dystrophin resulted in suppression of early PTP and LTP generated in the SC-CA1 collaterals of *mdx* mice. Mimicking the elevated levels of circulating IL-6 associated with this inflammatory disease and previously reported in *mdx* mice (Manning et al., 2014; Pelosi et al., 2015), exposure of hippocampal slices from dystrophin-expressing WT mice to IL-6, suppressed LTP, such that LTP now mimicked that in *mdx* mice. Moreover, intrathecal injection of neutralising IL-6R antibodies (24-h exposure) reversed the suppression of hippocampal LTP in *mdx* mice, implicating this cytokine in hippocampal dysfunction in the context of immune activation associated with loss of dystrophin.

Generally, in health, IL-6 supports processes involved in learning and memory, whereas in the context of inflammation, pathologically-elevated levels of IL-6 can have detrimental effects on mechanisms underpinning learning and memory formation (Bourgognon and Cavanagh, 2020). Indeed, mice over-expressing IL-6 have memory impairments (Heyser et al., 1997; Wei et al., 2012a, 2013) and others have reported that acute application of IL-6 suppressed both LTP and PTP (Li et al., 1997; Tancredi et al., 2000). Consistent with the reported central actions of IL-6, including modulation of immune function and energy metabolism, we observed modulatory effects of IL-6 on bioenergetics in different hippocampal regions. The most striking change was the suppression of basal respiration in the CA1, CA3 and DG regions with a concomitant rise in non-mitochondrial oxygen consumption. Given the regionally distinct functions of the pyramidal cell layers of the CA1 and CA3 regions, and the DG granule cells, it was interesting to observe different patterns of IL-6 and IL-6R expression, which may influence sensitivity to this neuromodulatory cytokine.

The absence of both Dp427 and Dp71 dystrophin isoforms from CA1, CA3 and DG regions of *mdx* mice was confirmed using immunofluorescence labelling, a finding that contrasted with strong dystrophin expression in the neuronal cell layers of WT hippocampal tissue. In agreement with the work of Moore & colleagues (Moore et al., 2002), LTP in the CA1 *stratum radiatum* following high frequency stimulation of SC-CA1 collaterals exhibited a significant decrease in the slope of fEPSPs in *mdx* compared to WT mice, which aligns with reported deficits in learning new tasks or storing spatial memories (Bagdatlioglu et al., 2020; Chaussenot et al., 2015; Vaillend et al., 1995, 2004). PTP, an early stage of synaptic plasticity, involving pre-synaptic changes in neurotransmitter release (Lauri et al., 2007), which occurs during the first few minutes of LTP induction, was suppressed in *mdx* tissue. Moreover, the maintenance phase of LTP (~1 h of recordings), which involves post-synaptic changes, indicative of reduced synaptic efficacy in the absence of dystrophin was also suppressed in *mdx* hippocampal slices.

As LTP is contingent upon tightly-regulated spatio-temporal control of intracellular calcium, and requires significant energy input (Olesen et al., 2020), we explored the importance of dystrophin in hippocampal mitochondrial function. In addition to powering cellular function, mitochondria act as sentinels, detecting cellular insults and orchestrating appropriate inflammatory responses (Li et al., 2013), a role likely to be important in inflammatory disorders, such as DMD. Maximal mitochondrial respiration is lacking in muscle biopsies from humans with DMD (Sperl et al., 1997) and mitochondria are unable to meet ATP demand in *mdx* mouse myocytes (Percival et al., 2013). Basal ATP demand in neurons accounts for ~20% of respiratory capacity (Jekabsons and Nicholls, 2004). However, we did not detect differences between basal respiration in unstimulated WT and *mdx* tissues in the CA1, CA3 or DG regions. Thus, at rest, basal mitochondrial respiratory function does not appear to be abnormal in dystrophic hippocampal neurons. When we examined maximal or uncoupled (using FCCP) cellular respiration, region-specific differences between unstimulated WT and *mdx* hippocampal tissue were evident. Maximal respiration was decreased in the *mdx* CA1 region compared to WT but higher in the CA3 region, where recurrent collateral projections associated with spatial working memory terminate (Le Duigou et al., 2014). Increased maximal respiration in this region may be required for the sustained neuronal activity needed to support working memory, which may put additional metabolic demands on this tissue in dystrophic mice.

Despite elevated levels of peripheral IL-6 (Manning et al., 2014), *Il6* gene and IL-6 protein levels were unchanged in whole hippocampal homogenates from *mdx* mice. Moreover, there was no evidence of gene upregulation of membrane-bound *Il6* receptors, *gp130*, the transmembrane protein which initiates the downstream signalling cascade or *STAT3*. This contrasts with the work of Jackson & colleagues, who

detected decreased *Il6* mRNA in hippocampal tissue, although they used *mdx*$^{\beta geo}$ mice, where all dystrophin isoforms have been ablated (Jackson et al., 2022). The caveat to using homogenised whole hippocampal tissue in these experiments is that differential, region-specific changes cannot be elucidated. While acknowledging the limitations of quantifying immunofluorescent staining of IL-6 and IL-6R expression, we did observe an increase in the relative intensity of IL-6 and IL-6R immunofluorescence in the CA1 and DG regions in *mdx* mice in comparison to WT. In contrast, expression of IL-6 protein was unchanged in the CA3 region of *mdx* hippocampal slices and IL-6R expression was decreased in dystrophic CA3 tissue. Reduced expression of IL-6Rs, and potentially decreased sensitivity to IL-6, in *mdx* CA3 region neurons is noteworthy, as CA3 is the site where theta-burst stimulation of the Schaffer collaterals induces LTP in CA1 neurons (Malenka and Nicoll, 1999). In contrast, both the CA1 and DG are likely to be more sensitive to the neuromodulatory actions of IL-6, although further region-specific protein quantification is warranted. Further research is also required to determine if loss of the dystrophin-dependant scaffold that anchors receptors and ion channels (Waite et al., 2012) is directly impacting upon expression of IL-6Rs, or if the region-specific changes are secondary to other CNS changes.

The potential neuromodulatory influence of IL-6 was explored, firstly in WT, dystrophin-expressing hippocampal slices. Consistent with overexpression of IL-6 resulting in broad memory impairments (Heyser et al., 1997; Wei et al., 2012b, 2013), we found that acute (1 h, in bath) exposure to IL-6 resulted in suppression of PTP in WT mice, although that change wasn't maintained for the course of the LTP recording. This may indicate that IL-6 modifies the early stages of LTP, that are reliant on pre-synaptic mechanisms, where IL-6Rα and gp130 are expressed (D'Arcangelo et al., 2000). In contrast, exposure to IL-6 had no impact on LTP generated in *mdx* mice, perhaps due to insensitivity to IL-6 caused by chronically elevated IL-6 (Pelosi et al., 2015). Indeed, our immunofluorescence data showed decreased expression of IL-6Rs in the *mdx* CA3 region, where the high frequency stimulation was applied, although further work is needed to confirm this.

IL-6 can modulate pathways associated with energetic metabolism (Mirabella et al., 2021), and despite the regional variability of expression of IL-6Rs, basal respiration levels were blunted in CA1, CA3 and DG regions of *mdx* hippocampal tissue acutely exposed to IL-6, which may have functional consequences during the induction of LTP. Interruption of the electron transport chain or decreased proton leak due to a reduction in the activity of uncoupling proteins may contribute to the reduction in basal respiration (Hill et al., 2012). Indeed, we observed decreased proton leak in all hippocampal regions exposed to IL-6. In *mdx* myocytes the capacity to synthesise ATP was reduced possibly due to low substrate availability, decreased mitochondrial mass or poor integrity of the electron transport chain (Percival et al., 2013). However, it is unlikely that ATP synthase was inhibited in hippocampal neurons, as ATP production was not significantly affected by IL-6. Spare respiratory capacity reflects the capacity of mitochondria to increase respiration in response to elevated ATP demand, but no differences were detected between strains in unstimulated or IL-6 exposed tissues. We detected increased proton leak from CA1 neurons compared to DG neurons in both WT and *mdx* hippocampi. However, this regional difference was not evident in tissues which had been exposed to IL-6, reflecting changes in neuronal bioenergetics induced by elevated levels of this cytokine. Coupling efficiency, the proportion of basal OCR used to drive ATP synthesis, was similar between strains and was not affected by exposure to IL-6. Finally, in all hippocampal regions, we noted a shift towards non-mitochondrial oxygen-consumption in *mdx* tissue after IL-6 exposure. Thus, some elements of bioenergetics, such as maximal respiration, were modified in the tissue derived from the pyramidal or granule cell layers of *mdx* mice. Moreover, the additional challenge of elevated levels of the pro-inflammatory cytokine, IL-6, further impacted upon respiratory function in *mdx* hippocampal regions.

Finally, we confirmed the importance of IL-6 in altered hippocampal synaptic plasticity related to loss of dystrophin, using *in vivo* inhibition of IL-6R-evoked signalling cascades in the CNS. In WT mice, where IL-6 is circulating at physiological levels, this intervention had no effect on the early or maintenance phases of hippocampal LTP. However, in dystrophin-deficient hippocampal tissue, where expression of IL-6 and IL-6Rs and cellular metabolism is altered, blocking IL-6 signalling resulted in enhancement of both early PTP and the maintenance phase of LTP. Thus, inhibition of IL-6 signalling in *mdx* mice resulted in LTP comparable to dystrophin-expressing WT LTP.

5. Conclusions

This investigation of hippocampal function in dystrophic *mdx* mice has revealed several findings that shed light on the functional role of neuronal dystrophin in the context of a disorder characterised by chronic inflammation, with elevated levels of IL-6. The high energy demand associated with synchronised spatio-temporal regulation of neurocircuitry underpinning learning-related processes, such as hippocampal LTP, require functional mitochondria. Thus, the observed dysregulation of cellular bioenergetics associated with loss of dystrophin may contribute to hippocampal dysfunction and subsequently negatively impact processes of learning and memory consolidation. Moreover, the pathophysiological impact of IL-6 was evidenced by suppression of WT LTP in the presence of IL-6 and the rescue of LTP in *mdx* mice following *in vivo* inhibition of central IL-6 signalling pathways. Thus, dystrophin deficiency was associated with altered cellular bioenergetics and suppressed LTP and we have demonstrated that IL-6 mediates some of these effects. These findings support a role for IL-6 as a contributary factor in cognitive deficits reported in disorders of dystrophin-deficiency, such as DMD.

CRediT authorship contribution statement

Kimberley A. Stephenson: Writing – review & editing, Formal analysis, Data curation. **Aaron Barron:** Writing – review & editing, Resources. **Mark G. Rae:** Writing – review & editing, Writing – original draft, Methodology, Investigation, Formal analysis, Data curation, Conceptualization. **Dervla O'Malley:** Writing – review & editing, Writing – original draft, Supervision, Resources, Project administration, Methodology, Investigation, Funding acquisition, Formal analysis, Data curation, Conceptualization.

Funding

This work was supported by fundings from the Health Research Board, Ireland. ILP-POR-2017-040.

Original data is available upon request.

Declaration of competing interest

The authors declare the following financial interests/personal relationships which may be considered as potential competing interests: Dervla O'Malley reports financial support was provided by Health Research Board Ireland. Dervla O'Malley reports equipment, drugs, or supplies was provided by Chugai Pharmaceutical Co., Ltd, Tokyo, Japan. If there are other authors, they declare that they have no known competing financial interests or personal relationships that could have appeared to influence the work reported in this paper.

Acknowledgements

We would like to acknowledge the additional technical supports provided by Dr B. Boland and Mr J. Radford University College Cork, Ireland.

Data availability

Data will be made available on request.

References

Anderson, J.L., Head, S.I., Rae, C., Morley, J.W., 2002. Brain function in Duchenne muscular dystrophy. Brain 125, 4–13.

Bagdatlioglu, E., Porcari, P., Greally, E., Blamire, A.M., Straub, V.W., 2020. Cognitive impairment appears progressive in the mdx mouse. Neuromuscul. Disord. 30, 368–388.

Banks, W.A., Kastin, A.J., Gutierrez, E.G., 1994. Penetration of interleukin-6 across the murine blood-brain barrier. Neurosci. Lett. 179, 53–56.

Bliss, T., Collingridge, G.L., 2019. Persistent memories of long-term potentiation and the N-methyl-d-aspartate receptor. Brain Neurosci Adv 3, 2398212819848213.

Bliss, T.V., Collingridge, G.L., 1993. A synaptic model of memory: long-term potentiation in the hippocampus. Nature 361, 31–39.

Bourgognon, J.M., Cavanagh, J., 2020. The role of cytokines in modulating learning and memory and brain plasticity. Brain Neurosci Adv 4, 2398212820979802.

Brunig, I., Suter, A., Knuesel, I., Luscher, B., Fritschy, J.M., 2002. GABAergic terminals are required for postsynaptic clustering of dystrophin but not of GABA(A) receptors and gephyrin. J. Neurosci. 22, 4805–4813.

Budzinska, M., Zimna, A., Kurpisz, M., 2021. The role of mitochondria in Duchenne muscular dystrophy. J. Physiol. Pharmacol. 72.

Chaussenot, R., Edeline, J.M., Le Bec, B., El Massioui, N., Laroche, S., Vaillend, C., 2015. Cognitive dysfunction in the dystrophin-deficient mouse model of Duchenne muscular dystrophy: a reappraisal from sensory to executive processes. Neurobiol. Learn. Mem. 124, 111–122.

Chieffo, D.P.R., Moriconi, F., Mastrilli, L., Lino, F., Brogna, C., Coratti, G., Altobelli, M., Massaroni, V., Norcia, G., Ferraroli, E., Lucibello, S., Pane, M., Mercuri, E., 2022. Language development in preschool duchenne muscular dystrophy boys. Brain Sci. 12.

Culligan, K., Ohlendieck, K., 2002. Diversity of the brain dystrophin-glycoprotein complex. J. Biomed. Biotechnol. 2, 31–36.

D'Arcangelo, G., Tancredi, V., Onofri, F., D'Antuono, M., Giovedi, S., Benfenati, F., 2000. Interleukin-6 inhibits neurotransmitter release and the spread of excitation in the rat cerebral cortex. Eur. J. Neurosci. 12, 1241–1252.

Felisari, G., Martinelli Boneschi, F., Bardoni, A., Sironi, M., Comi, G.P., Robotti, M., Turconi, A.C., Lai, M., Corrao, G., Bresolin, N., 2000. Loss of Dp140 dystrophin isoform and intellectual impairment in Duchenne dystrophy. Neurology 55, 559–564.

Haenggi, T., Soontornmalai, A., Schaub, M.C., Fritschy, J.M., 2004. The role of utrophin and Dp71 for assembly of different dystrophin-associated protein complexes (DPCs) in the choroid plexus and microvasculature of the brain. Neuroscience 129, 403–413.

Heyser, C.J., Masliah, E., Samimi, A., Campbell, I.L., Gold, L.H., 1997. Progressive decline in avoidance learning paralleled by inflammatory neurodegeneration in transgenic mice expressing interleukin 6 in the brain. Proc. Natl. Acad. Sci. U.S.A. 94, 1500–1505.

Hill, B.G., Benavides, G.A., Lancaster Jr., J.R., Ballinger, S., Dell'Italia, L., Jianhua, Z., Darley-Usmar, V.M., 2012. Integration of cellular bioenergetics with mitochondrial quality control and autophagy. Biol. Chem. 393, 1485–1512.

Hinton, V.J., De Vivo, D.C., Nereo, N.E., Goldstein, E., Stern, Y., 2001. Selective deficits in verbal working memory associated with a known genetic etiology: the neuropsychological profile of duchenne muscular dystrophy. J. Int. Neuropsychol. Soc. 7, 45–54.

Hinton, V.J., Fee, R.J., De Vivo, D.C., Goldstein, E., 2007. Poor facial affect recognition among boys with duchenne muscular dystrophy. J. Autism Dev. Disord. 37, 1925–1933.

Jackson, T., Seifi, M., Gorecki, D.C., Swinny, J.D., 2022. Specific dystrophins selectively associate with inhibitory and excitatory synapses of the mouse cerebellum and their loss alters expression of P2X7 purinoceptors and pro-inflammatory mediators. Cell. Mol. Neurobiol. 42, 2357–2377.

Jekabsons, M.B., Nicholls, D.G., 2004. In situ respiration and bioenergetic status of mitochondria in primary cerebellar granule neuronal cultures exposed continuously to glutamate. J. Biol. Chem. 279, 32989–33000.

Knuesel, I., Bornhauser, B.C., Zuellig, R.A., Heller, F., Schaub, M.C., Fritschy, J.M., 2000. Differential expression of utrophin and dystrophin in CNS neurons: an in situ hybridization and immunohistochemical study. J. Comp. Neurol. 422, 594–611.

Knuesel, I., Mastrocola, M., Zuellig, R.A., Bornhauser, B., Schaub, M.C., Fritschy, J.M., 1999. Short communication: altered synaptic clustering of GABAA receptors in mice lacking dystrophin (mdx mice). Eur. J. Neurosci. 11, 4457–4462.

Kueh, S.L., Head, S.I., Morley, J.W., 2008. GABA(A) receptor expression and inhibitory post-synaptic currents in cerebellar Purkinje cells in dystrophin-deficient mdx mice. Clin. Exp. Pharmacol. Physiol. 35, 207–210.

Lauri, S.E., Palmer, M., Segerstrale, M., Vesikansa, A., Taira, T., Collingridge, G.L., 2007. Presynaptic mechanisms involved in the expression of STP and LTP at CA1 synapses in the hippocampus. Neuropharmacology 52, 1–11.

Le Duigou, C., Simonnet, J., Telenczuk, M.T., Fricker, D., Miles, R., 2014. Recurrent synapses and circuits in the CA3 region of the hippocampus: an associative network. Front. Cell. Neurosci. 7, 262.

Li, A.J., Katafuchi, T., Oda, S., Hori, T., Oomura, Y., 1997. Interleukin-6 inhibits long-term potentiation in rat hippocampal slices. Brain Res. 748, 30–38.

Li, X., Fang, P., Mai, J., Choi, E.T., Wang, H., Yang, X.F., 2013. Targeting mitochondrial reactive oxygen species as novel therapy for inflammatory diseases and cancers. J. Hematol. Oncol. 6, 19.

Lidov, H.G., Byers, T.J., Kunkel, L.M., 1993. The distribution of dystrophin in the murine central nervous system: an immunocytochemical study. Neuroscience 54, 167–187.

Lidov, H.G., Byers, T.J., Watkins, S.C., Kunkel, L.M., 1990. Localization of dystrophin to postsynaptic regions of central nervous system cortical neurons. Nature 348, 725–728.

Liu, Y., Beyer, A., Aebersold, R., 2016. On the dependency of cellular protein levels on mRNA abundance. Cell 165, 535–550.

Lopez, J.R., Kolster, J., Uryash, A., Esteve, E., Altamirano, F., Adams, J.A., 2018. Dysregulation of intracellular Ca(2+) in dystrophic cortical and hippocampal neurons. Mol. Neurobiol. 55, 603–618.

Malenka, R.C., Nicoll, R.A., 1999. Long-term potentiation–a decade of progress? Science 285 (5435), 1870–1874.

Manning, J., Kulbida, R., Rai, P., Jensen, L., Bouma, J., Singh, S.P., O'Malley, D., Yilmazer-Hanke, D., 2014. Amitriptyline is efficacious in ameliorating muscle inflammation and depressive symptoms in the mdx mouse model of Duchenne muscular dystrophy. Exp. Physiol. 99, 1370–1386.

Mareedu, S., Million, E.D., Duan, D., Babu, G.J., 2021. Abnormal calcium handling in duchenne muscular dystrophy: mechanisms and potential therapies. Front. Physiol. 12, 647010.

McDonald, C.M., Henricson, E.K., Abresch, R.T., Duong, T., Joyce, N.C., Hu, F., Clemens, P.R., Hoffman, E.P., Cnaan, A., Gordish-Dressman, H., Investigators, C., 2018. Long-term effects of glucocorticoids on function, quality of life, and survival in patients with Duchenne muscular dystrophy: a prospective cohort study. Lancet 391, 451–461.

Mirabella, F., Desiato, G., Mancinelli, S., Fossati, G., Rasile, M., Morini, R., Markicevic, M., Grimm, C., Amegandjin, C., Termanini, A., Peano, C., Kunderfranco, P., di Cristo, G., Zerbi, V., Menna, E., Lodato, S., Matteoli, M., Pozzi, D., 2021. Prenatal interleukin 6 elevation increases glutamatergic synapse density and disrupts hippocampal connectivity in offspring. Immunity 54, 2611–2631 e2618.

Moore, S.A., Saito, F., Chen, J., Michele, D.E., Henry, M.D., Messing, A., Cohn, R.D., Ross-Barta, S.E., Westra, S., Williamson, R.A., Hoshi, T., Campbell, K.P., 2002. Deletion of brain dystroglycan recapitulates aspects of congenital muscular dystrophy. Nature 418, 422–425.

Moore, T.M., Lin, A.J., Strumwasser, A.R., Cory, K., Whitney, K., Ho, T., Ho, T., Lee, J.L., Rucker, D.H., Nguyen, C.Q., Yackly, A., Mahata, S.K., Wanagat, J., Stiles, L., Turcotte, L.P., Crosbie, R.H., Zhou, Z., 2020. Mitochondrial dysfunction is an early consequence of partial or complete dystrophin loss in mdx mice. Front. Physiol. 11, 690.

Nardes, F., Araujo, A.P., Ribeiro, M.G., 2012. Mental retardation in Duchenne muscular dystrophy. J. Pediatr. 88, 6–16.

Nico, B., Frigeri, A., Nicchia, G.P., Corsi, P., Ribatti, D., Quondamatteo, F., Herken, R., Girolamo, F., Marzullo, A., Svelto, M., Roncali, L., 2003. Severe alterations of endothelial and glial cells in the blood-brain barrier of dystrophic mdx mice. Glia 42, 235–251.

Okazaki, M., Yamada, Y., Nishimoto, N., Yoshizaki, K., Mihara, M., 2002. Characterization of anti-mouse interleukin-6 receptor antibody. Immunol. Lett. 84, 231–240.

Olesen, M.A., Torres, A.K., Jara, C., Murphy, M.P., Tapia-Rojas, C., 2020. Premature synaptic mitochondrial dysfunction in the hippocampus during aging contributes to memory loss. Redox Biol. 34, 101558.

Pelosi, L., Berardinelli, M.G., Forcina, L., Spelta, E., Rizzuto, E., Nicoletti, C., Camilli, C., Testa, E., Catizone, A., De Benedetti, F., Musaro, A., 2015. Increased levels of interleukin-6 exacerbate the dystrophic phenotype in mdx mice. Hum. Mol. Genet. 24, 6041–6053.

Percival, J.M., Siegel, M.P., Knowels, G., Marcinek, D.J., 2013. Defects in mitochondrial localization and ATP synthesis in the mdx mouse model of Duchenne muscular dystrophy are not alleviated by PDE5 inhibition. Hum. Mol. Genet. 22, 153–167.

Rae, M.G., O'Malley, D., 2016. Cognitive dysfunction in Duchenne muscular dystrophy: a possible role for neuromodulatory immune molecules. J. Neurophysiol. 116, 1304–1315.

Ricotti, V., Mandy, W.P., Scoto, M., Pane, M., Deconinck, N., Messina, S., Mercuri, E., Skuse, D.H., Muntoni, F., 2016. Neurodevelopmental, emotional, and behavioural problems in Duchenne muscular dystrophy in relation to underlying dystrophin gene mutations. Dev. Med. Child Neurol. 58, 77–84.

Sekiguchi, M., Zushida, K., Yoshida, M., Maekawa, M., Kamichi, S., Yoshida, M., Sahara, Y., Yuasa, S., Takeda, S., Wada, K., 2009. A deficit of brain dystrophin impairs specific amygdala GABAergic transmission and enhances defensive behaviour in mice. Brain 132, 124–135.

Sesay, A.K., Errington, M.L., Levita, L., Bliss, T.V., 1996. Spatial learning and hippocampal long-term potentiation are not impaired in mdx mice. Neurosci. Lett. 211, 207–210.

Snow, W.M., Anderson, J.E., Jakobson, L.S., 2013. Neuropsychological and neurobehavioral functioning in Duchenne muscular dystrophy: a review. Neurosci. Biobehav. Rev. 37, 743–752.

Sperl, W., Skladal, D., Gnaiger, E., Wyss, M., Mayr, U., Hager, J., Gellerich, F.N., 1997. High resolution respirometry of permeabilized skeletal muscle fibers in the diagnosis of neuromuscular disorders. Mol. Cell. Biochem. 174, 71–78.

Swandulla, D., Hans, M., Zipser, K., Augustine, G.J., 1991. Role of residual calcium in synaptic depression and posttetanic potentiation: fast and slow calcium signaling in nerve terminals. Neuron 7, 915–926.

Tadayoni, R., Rendon, A., Soria-Jasso, L.E., Cisneros, B., 2012. Dystrophin Dp71: the smallest but multifunctional product of the Duchenne muscular dystrophy gene. Mol. Neurobiol. 45, 43–60.
Tancredi, V., D'Antuono, M., Cafe, C., Giovedi, S., Bue, M.C., D'Arcangelo, G., Onofri, F., Benfenati, F., 2000. The inhibitory effects of interleukin-6 on synaptic plasticity in the rat hippocampus are associated with an inhibition of mitogen-activated protein kinase ERK. J. Neurochem. 75, 634–643.
Tulangekar, A., Sztal, T.E., 2021. Inflammation in duchenne muscular dystrophy-exploring the role of neutrophils in muscle damage and regeneration. Biomedicines 9.
Underwood, E., Redell, J.B., Zhao, J., Moore, A.N., Dash, P.K., 2020. A method for assessing tissue respiration in anatomically defined brain regions. Sci. Rep. 10, 13179.
Vaillend, C., Billard, J.M., 2002. Facilitated CA1 hippocampal synaptic plasticity in dystrophin-deficient mice: role for GABAA receptors? Hippocampus 12, 713–717.
Vaillend, C., Billard, J.M., Laroche, S., 2004. Impaired long-term spatial and recognition memory and enhanced CA1 hippocampal LTP in the dystrophin-deficient Dmd(mdx) mouse. Neurobiol. Dis. 17, 10–20.
Vaillend, C., Rendon, A., Misslin, R., Ungerer, A., 1995. Influence of dystrophin-gene mutation on mdx mouse behavior. I. Retention deficits at long delays in spontaneous alternation and bar-pressing tasks. Behav. Genet. 25, 569–579.
Verhaeg, M., Adamzek, K., van de Vijver, D., Putker, K., Engelbeen, S., Wijnbergen, D., Overzier, M., Suidgeest, E., van der Weerd, L., Aartsma-Rus, A., van Putten, M., 2024. Learning, memory and blood-brain barrier pathology in Duchenne muscular dystrophy mice lacking Dp427, or Dp427 and Dp140. Gene Brain Behav. 23, e12895.
Waite, A., Brown, S.C., Blake, D.J., 2012. The dystrophin-glycoprotein complex in brain development and disease. Trends Neurosci. 35, 487–496.
Waite, A., Tinsley, C.L., Locke, M., Blake, D.J., 2009. The neurobiology of the dystrophin-associated glycoprotein complex. Ann. Med. 41, 344–359.
Wei, H., Alberts, I., Li, X., 2013. Brain IL-6 and autism. Neuroscience 252, 320–325.
Wei, H., Chadman, K.K., McCloskey, D.P., Sheikh, A.M., Malik, M., Brown, W.T., Li, X., 2012a. Brain IL-6 elevation causes neuronal circuitry imbalances and mediates autism-like behaviors. Biochim. Biophys. Acta 1822, 831–842.
Wei, H., Mori, S., Hua, K., Li, X., 2012b. Alteration of brain volume in IL-6 overexpressing mice related to autism. Int. J. Dev. Neurosci. 30, 554–559.
West, M.J., Slomianka, L., Gundersen, H.J., 1991. Unbiased stereological estimation of the total number of neurons in thesubdivisions of the rat hippocampus using the optical fractionator. Anat. Rec. 231, 482–497.
Wu, M., Neilson, A., Swift, A.L., Moran, R., Tamagnine, J., Parslow, D., Armistead, S., Lemire, K., Orrell, J., Teich, J., Chomicz, S., Ferrick, D.A., 2007. Multiparameter metabolic analysis reveals a close link between attenuated mitochondrial bioenergetic function and enhanced glycolysis dependency in human tumor cells. Am. J. Physiol. Cell Physiol. 292 (1), C125–136.